Probabilistic Aerothermal Design of Gas Turbine Combustors

by

Sean Darien Bradshaw

S.B., Massachusetts Institute of Technology (2000)
S.M., Massachusetts Institute of Technology (2002)

Submitted to the Department of Aeronautics and Astronautics
in partial fulfillment of the requirements for the degree of

Doctor of Philosophy in Aeronautics and Astronautics

at the

MASSACHUSETTS INSTITUTE OF TECHNOLOGY

June 2006

© Massachusetts Institute of Technology 2006. All rights reserved.

Author .....
Department of Aeronautics and Astronautics
May 26, 2006

Certified by .....
Ian Waitz
Professor of Aeronautics and Astronautics
Thesis Supervisor

Certified by .....
Edward Greitzer
Professor of Aeronautics and Astronautics

Certified by .....
David Darmofal
Associate Professor of Aeronautics and Astronautics

Accepted by .....
Jaime Peraire
Chairman, Department Committee on Graduate Students

MASSACHUSETTS INSTITUTE OF TECHNOLOGY
JUL 10 2006
LIBRARIES

ARCHIVES

Probabilistic Aerothermal Design of Gas Turbine Combustors

by

Sean Darien Bradshaw

Submitted to the Department of Aeronautics and Astronautics
on May 26, 2006, in partial fulfillment of the
requirements for the degree of
Doctor of Philosophy in Aeronautics and Astronautics

Abstract

This thesis presents a probability-based framework for assessing the impact of manufacturing variability on combustor liner durability. Simplified models are used to link combustor liner life, liner temperature variability, and the effects of manufacturing variability. A probabilistic analysis is then applied to the simplified models to estimate the combustor life distribution. The material property and liner temperature variations accounted for approximately 80 percent and 20 percent, respectively, of the combustor life variability. Furthermore, the typical combustor life was found to be approximately 20 percent less than the life estimated using deterministic methods for these combustors, and the probability that a randomly selected combustor will fail earlier than predicted using deterministic methods is approximately 80 percent. Finally, the application of a sensitivity analysis to a surrogate model for the life identified the leading drivers of the minimum combustor life and the typical combustor life as the material property variability and the variability of the near-wall combustor gas temperature, respectively.

Thesis Supervisor: Ian Waitz
Title: Professor of Aeronautics and Astronautics

Acknowledgments

I would like to thank Professor Ian Waitz, who provided me with a tremendous amount of guidance and support during my doctoral studies. I would also like to thank my doctoral committee members, Professor Edward Greitzer and Professor David Darmofal, for their insightful critiques of this research. I would like to thank General Electric Aircraft Engines for providing me with the data necessary to complete this research. Specifically, I would like to thank Aureen Currin, Harris Abramson, Frank Lastrina, Mark Shaw, Steve Stephens, and Joe Monty for their guidance.

I would like to thank my family and friends for their support during the last four years. In particular, I could never have succeeded without the love, patience, and understanding of my wife, Janelle. Finally, thank you to Brittany for always putting a smile on my face.

This research was supported by a Ford Foundation Pre-doctoral Fellowship.

Contents

1 Introduction **13**

1.1 Motivation 13
1.2 Literature Review 14
1.3 Research Objectives 16
1.4 Thesis Overview 16
1.5 Contributions 17

2 Combustor Modeling **19**

2.1 Introduction 19
2.2 Network Flow Analysis 24
2.3 Temperature Field Analysis 27
2.3.1 Bulk Gas Temperature 27
2.3.2 Near-Wall Gas Temperature 32
2.3.3 Film Temperature 32
2.3.4 Deterministic Analysis 33
2.4 Heat Transfer Analysis 34
2.5 Liner Life Analysis 36
2.5.1 Crack Initiation Life 36
2.5.2 Crack Propagation Life 37
2.5.3 Total Life 37
2.6 Summary 37

3 Impact of Manufacturing Variability on Combustor Liner Durability **39**

3.1 Introduction 39
3.2 Manufacturing Variability 39
3.2.1 Random Variables 39
3.2.2 Nested Classes of Variability 39
3.2.3 Hierarchical Analysis 43
3.3 Model Assessment 44
3.3.1 Combustor Outlet Bulk Gas Temperatures 44
3.3.2 Combustor Liner Temperatures 46
3.3.3 Discussion 47
3.3.4 Combustor Liner Life 49
3.4 Conclusions 55

4 Sensitivity Analysis **57**
4.1 Introduction . . . 57
4.2 Response Surface Analysis . . . 57
4.2.1 Application to Monte Carlo Data . . . 59
4.3 Impact of Tightening Manufacturing Tolerances . . . 60
4.3.1 Case 1: 90-percent tolerance reduction . . . 60
4.3.2 Case 2: 10-percent tolerance reduction . . . 61
4.4 Impact of Opening Manufacturing Tolerances . . . 66
4.5 Conclusions . . . 69

5 Summary and Recommendations **71**
5.1 Summary . . . 71
5.2 Recommendations for Future Work . . . 72
5.2.1 Analytical Modeling of the Combustor Mixedness . . . 72
5.2.2 Impact of Operational Variability on Combustor Liner Durability . . 72
5.2.3 Impact of Manufacturing Variability on Hot-Streak Migration 72
5.2.4 Probability-Based Combustion System Optimization . . . 72
5.2.5 Study of Material Property Variability versus Measurement Error . 73

A Crack Initiation Life Modeling **75**
A.1 Universal Slopes Method . . . 75
A.2 Young's Modulus . . . 76
A.3 Coefficient of Thermal Expansion . . . 76
A.4 Ultimate Tensile Stress . . . 76
A.5 Ductility . . . 77
A.6 Solution Procedure . . . 77
A.7 Crack Initiation Life Curve . . . 78

B Crack Propagation Life Modeling **79**
B.1 Constant Temperature Crack Growth . . . 79
B.2 Variable Temperature Crack Growth . . . 80

C JP-8 Chemical Kinetic Mechanism **81**
C.1 Chemical Mechanism . . . 81
C.2 Reaction Rate Constant . . . 81

D Probability Fundamentals **83**
D.1 Random Variables . . . 83
D.2 Gaussian Distribution . . . 84
D.3 Log-normal Distribution . . . 84
D.4 Weibull Distribution . . . 84

Bibliography **86**

List of Figures

1-1 Combustor liner distress (Source: A. Mascarenas, *Delta Airlines*) 13

2-1 Probabilistic modeling framework for assessing the impact of manufacturing variability on combustor liner temperature and liner life. 20
2-2 Sketch of a combustor with I panels. 23
2-3 Sketch of a combustor with J sectors, or cup sections. 23
2-4 Sketch of the mass flows crossing the combustor liner. 24
2-5 Sketch of the combustor mass flow circuit. $\dot{m}_c$ is the total combustor mass flow, $G_{film,i,j}$ is the flow conductance for the film flow, $G_{dilution,i,j}$ is the flow conductance for the dilution mass flow, $G_{air,j}$ is the conductance for the dome flow, and f_c is the mass flow-pressure drop function. 26
2-6 Sketch of a lumped-parameter model for the combustor temperature field. The temperature field is separated into three driving temperatures and applied in a one-dimensional heat transfer analysis. These temperatures are the bulk gas temperature, the near-wall gas temperature, and the cooling film temperature. 27
2-7 Application of a well-stirred reactor analysis to estimate of the bulk gas temperature in the i^{th} panel and j^{th} cup section. The reactor inlets consist of the air admission ports at the dome, the outer liner, and the inner liner. The reactor outlet faces the combustor outlet. 29
2-8 Contour plot of the estimation error of the surrogate model. The ordinate is the compressor discharge temperature divided by a reference temperature. The abscissa is the bulk gas equivalence ratio. The error is determined by taking difference between the response surface estimate and the CHEMKIN estimate, dividing the difference by the CHEMKIN estimate, and then taking the absolute value of the quotient. The nominal equivalence ratios for combustors A and B are shown in the contour plot. 31
2-9 Influence of mixedness parameter on radial temperature gradients by panel. g_2 is plotted vs. x_c/L_c for $\zeta_{i,j} = 2.0$. 33
2-10 Lumped-parameter analysis of combustor temperature field for combustors A and B. The gas temperature normalized by the compressor discharge air temperature vs. the panel number is plotted in this figure. 34
2-11 Sketch of a combustor liner wall. 35
2-12 Crack Initiation Life Curves 36

3-1 Random variables 40
3-2 Fuel injector flow curve: mass flow vs. pressure drop 41

3-3 Hierarchical analysis for 'M' combustors and 'J' cup sections at sea-level, hot-day, take-off operating condition. 43
3-4 Combustor A outlet bulk temperature variability 45
3-5 Combustor B outlet bulk temperature variability 45
3-6 Combustor A liner temperatures 48
3-7 Combustor B liner temperatures 48
3-8 Case I (without material property variability): combustor A life PDF . . . 50
3-9 Case I (without material property variability): combustor A life CDF on a Weibull scale 50
3-10 Case I (without material property variability): combustor B life PDF 51
3-11 Case I (without material property variability): combustor B life CDF on a Weibull scale 51
3-12 Case II (with material property variability): combustor A PDF 53
3-13 Case II (with material property variability): combustor A CDF on a Weibull scale 53
3-14 Case II (with material property variability): combustor B life PDF 54
3-15 Case II (with material property variability): combustor B life CDF on a Weibull scale 54

4-1 Combustor A: B_1 life change for 90 percent tolerance decrease. 62
4-2 Combustor A: B_{50} life change for 90 percent tolerance decrease. 62
4-3 Combustor B: B_1 life change for 90 percent tolerance decrease. 63
4-4 Combustor B: B_{50} life change for 90 percent tolerance decrease. 63
4-5 Combustor A: B_1 life change for 10 percent tolerance decrease. 64
4-6 Combustor A: B_{50} life change for 10 percent tolerance decrease. 64
4-7 Combustor B: B_1 life change for 10 percent tolerance decrease. 65
4-8 Combustor B: B_{50} life change for 10 percent tolerance decrease. 65
4-9 Combustor A: B_1 life change for 10 percent tolerance increase. 67
4-10 Combustor A: B_{50} life change for 10 percent tolerance increase. 67
4-11 Combustor B: B_1 life change for 10 percent tolerance increase. 68
4-12 Combustor B: B_{50} life change for 10 percent tolerance increase. 68

A-1 Crack initiation life model: Universal Slopes Method 78

List of Tables

2.1 Random Input Variables 21
2.2 Random Output Variables 21
2.3 Deterministic Input Parameters 21

3.1 Comparative Analysis of Combustor B Life 55

4.1 Sensitivity Analysis: Tightening Tolerances 60

C.1 JP-8 Chemical Kinetic Mechanism 82

Chapter 1

Introduction

1.1 Motivation

The lifetime of a gas turbine combustor is typically limited by the durability of its liner, the structure that surrounds the high-temperature combustion products. The goal of the combustor thermal design process is to ensure that the liner temperatures do not exceed a maximum value set by metallurgical limits while minimizing the amount of film cooling air used in the process. Liner temperatures exceeding this limit hasten the onset of cracking and buckling, as shown in Figure 1-1 [1]. These forms of distress increase the number of unscheduled engine removals, which cause the maintenance and repair costs of the engine to rise.

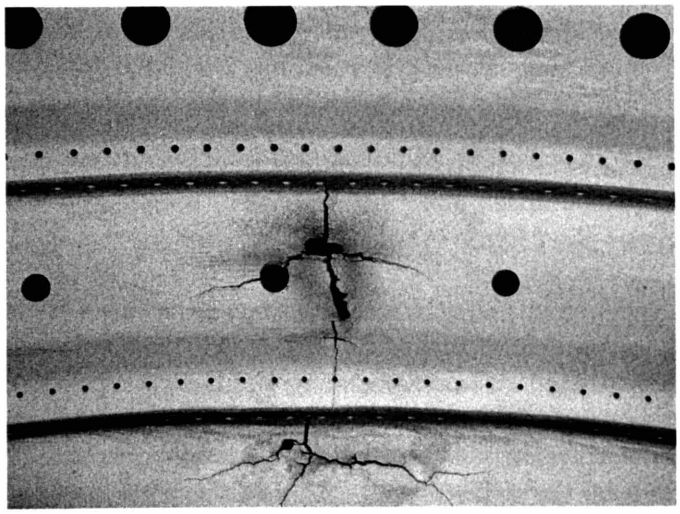

Figure 1-1: Combustor liner distress (Source: A. Mascarenas, *Delta Airlines*)

The gas turbine combustor must satisfy several competing objectives along with its durability requirements: performance, stability, pattern factor, emissions, and affordability. These requirements present several technical challenges during the design, manufacturing, and service phases of each new product. The primary function of the combustor is to efficiently convert the chemical energy stored in the fuel into internal energy. During this process, the combustor must provide a stable flame over a wide range of operating points.

Futhermore, lower specific fuel consumption requirements require higher turbine inlet temperatures and operating pressures. The temperatures in the combustor must also increase in order to deliver these elevated turbine inlet temperatures. Higher temperatures and pressures in the combustion chamber increase the radiative and convective loads to the liner walls. Stricter emissions standards necessitate the increased allocation of compressor discharge air to the primary zone [2]. As a result, a decreased amount of film cooling air is available to cool the liner. The turbine durability requirements result in increased pattern factor at the combustor outlet. Consequently, the amount of film cooling air used is decreased and the liner durability is adversely impacted. Moreover, the combustor life requirements have increased as the operating temperatures of the thermodynamic cycle have risen during the past few decades. Lastly, the combustor must also be manufactured and maintained at low cost while satisfying this litany of requirements.

A combination of analytical tools and rig tests is necessary in order to ensure the combustor satisfies its durability and other requirements. However, variability arising from imperfect manufacturing processes introduces uncertainty into the deterministic quantification of combustor liner life. The computational expense of the high-fidelity numerical tools typically used in combustor design prohibits the use of probabilistic methods with these tools. Moreover, the connections between the structural reliability, aerothermal variability, and manufacturing variability are seldom made due to the complexity of the task. In particular, causal relationships are not typically established among the sources of manufacturing variability, the liner temperature, and the liner life. Absence of these relationships prohibits an understanding of the extent to which the effects of manufacturing variability impact the combustor liner life. As a result, the impact of manufacturing variability is accounted for by making conservative assumptions and adopting design margins based on experience with similar products. These approaches may yield combustors that are overdesigned in order to meet one requirement (i.e. structural reliability) while yielding combustors that are suboptimal with respect to the other aspects of the design (i.e. performance, emissions, affordability).

1.2 Literature Review

Probability-based design and analysis methods have been used to assess the structural reliability of aerospace products for over three decades [4]. These techniques mitigate the conservatism of margin-based risk assessment methods by directly estimating part failure rates. These methods primarily focus on probabilistic analysis of the structural durability without accounting for the effects of aerothermal variability.

An early approach to the reliability analysis of fatigue life used the strain-life method [5]. This method consists of relating the applied stress to the lifetime of the part. This physical relationship is typically a strain-life curve derived from experiment. The maximum stress of the part is determined from a structural analysis. Then, the lifetime of the part is estimated using this maximum stress as an input to the strain-life relation.

An alternative approach to fatigue lifetime prediction is to quantify the impact of variability on the fracture mechanics. Millwater et. al. [6] implemented a probabilistic structural analysis program for predicting the crack propagation life while accounting for the effects of variability. Besterfield et. al. applied a probabilistic finite element analysis in order to estimate the crack growth [7]. Wu et. al. applied three stochastic fatigue crack growth models to study the impact of variability on the crack propagation life[11]. These

three crack growth models were a Markov chain model, Yang's power law, and a polynomial model.

The Monte Carlo method is a simulation tool for solving a wide array of mathematical problems [39]. Within the context of probabilistic durability analysis, this method is used to propagate the effects of variability to the fatigue life distribution. The Monte Carlo method contains several steps. The first step consists of forming a set a random variables using a random number generator. Second, the input values are randomly sampled from these distributions and applied to a physical model to estimate the output. This process is repeated until all of the points in the input distributions have been sampled. An advantage of the Monte Carlo method is its convergence rate is independent of the number of input parameters. A disadvantage of using this technique, however, is its slow rate of convergence. In particular, the convergence rate is inversely proportional to the square root of the number of trials.

Approximate techniques, such as the first-order reliability method (FORM), can be used to decrease the computational cost of reliability prediction [9]. FORM consists of defining a limit state function for the fatigue failure, performing a nonlinear optimization on the failure boundary in order to estimate a reliability index, and then estimating the probability of failure [8, 9, 10]. The limit state function in FORM is a linearized functional relationship between the fatigue life and the random inputs. This relation is either known prior to the statistical analysis or derived from a Design of Experiments (DoE).

Although these probability-based tools are widely used, there is little work on aerothermal design and analysis with variability. Garzon and Darmofal [12] proposed a probabilistic modeling methodology for quantifying the impact of geometric variability on compressor aerodynamic performance. This analysis focused on a flank-milled integrally-bladed rotor. A principal components analysis of the compressor blade surface measurements was used to derive models representing the effects of geometric variability. These variations were propagated through physical models of the compressor using a Monte Carlo analysis. The physical models consisted of a compressible, viscous blade passage model and a mean-line multistage compressor model. The outputs were distributions of loss, turning angle, compressor efficiency, and compressor pressure ratio. The authors showed that the effects of geometric variability they examined could reduce overall mean compressor efficiency by approximately one percent.

Sidwell and Darmofal [13] proposed a methodology for quantifying the impact of manufacturing variability on turbine blade cooling flow and oxidation life. The authors applied a network flow model to the cooling flow system in order to causally link key design parameters to the blade cooling mass flow. These parameters were represented by independent, normally-distributed random variables. The mean values and standard deviations were derived from the nominal design values and their tolerances, respectively. The authors identified the key driver of oxidation life to be the blade flow passage area using a sensitivity analysis. A selective assembly method was applied as a means of increasing the minimum life of a row of blades.

Mavris and Roth [14] proposed a general robust design methodology for the High Speed Civil Transport (HSCT) impingement-cooled combustor liner. The authors used a finite element model to estimate the liner thermal loads deterministically. Using Design of Experiments (DoE) techniques, they assembled a response surface equation (RSE) for liner temperature as a function of several key combustor design parameters. The authors showed that impingement hole spacing and the thermal barrier coating (TBC) thickness were the key drivers of liner temperature variance.

Mavris and Roth represented the variability of aerothermal parameters such as the hot-side convection coefficient, the compressor discharge temperature, and the adiabatic flame temperature as triangular probability density functions. The first and second moments of these distributions were based on design experience. The triangular distribution was chosen because the true natures of the probability distributions for these parameters were not known. As a result, causal relationships between these distributions and the geometric variability of the combustor were not established nor were inferences about the impact of the combustor liner temperature variability on the life distribution made. Finally, the authors did not provide a comparison between wall temperature measurements from a combustor rig data and the probabilistic model estimate.

1.3 Research Objectives

The main objectives of the work reported in this thesis are:

- To develop a simplified combustor model that links the effects of manufacturing variability, combustor liner temperature, and combustor liner life.
- To quantify the impact of manufacturing variability on low-cycle fatigue life using a probabilistic analysis.
- To identify the leading drivers of combustor liner low-cycle fatigue life using a sensitivity analysis.

1.4 Thesis Overview

This thesis presents a probability-based framework for quantifying the impact of manufacturing variability on combustor liner life. This framework consists of three major parts: a combustor model, a probabilistic analysis, and a sensitivity analysis. These parts are summarized in this section.

Chapter 2 presents a simplified model for estimating the combustor liner low-cycle fatigue life distribution. The model establishes causal relationships among a set of design parameters, the liner temperature, and the liner life. The model elements include a network flow analysis, a well-stirred reactor analysis, a lumped-parameter analysis of the combustor temperature field, a liner heat transfer analysis, and a low-cycle fatigue life analysis.

Chapter 3 introduces a probability-based framework for quantifying the impact of manufacturing variability on combustor liner durability. The probabilistic framework is applied to two combustors used on commercial aircraft engines. Several design parameters are modeled as independent, normally-distributed random variables. The mean values are determined from the nominal design specifications. The standard deviations are determined from manufacturing tolerances and other design specifications. The model was assessed by comparing probabilistic estimates of the liner temperature and liner life to wall temperature measurements and field failure data.

Chapter 4 proposes a methodology for determining the leading drivers of liner life. A regression analysis is performed to form a surrogate model for the life. Then, a sensitivity analysis is applied to this model in order to identify the leading drivers of the liner life for these combustors. The impact of changing the variability of the random inputs on combustor life is quantified.

1.5 Contributions

The main contributions of this thesis are:

- The development of a simplified combustor model that links manufacturing variability, aerothermal variability, and structural reliability. In particular, the model relates the effects of manufacturing variability of the liner, fuel mass flow variability, and air swirler mass flow variability to the bulk gas temperature at the combustor outlet, to the liner temperature, and to the liner life. The simplified model model consists of several main elements: network flow analysis, a well-stirred reactor analysis, a combustor temperature field analysis, a liner heat transfer analysis, and a low-cycle fatigue life analysis.

- Probabilistic assessment of the impact of fuel flow variability and air swirler flow variability on bulk gas temperature variability at the combustor outlet. The probabilistic estimate of the bulk gas temperature variability at the outlet was consistent with outlet temperature measurements obtained from a combustor rig test.

- Application of a probabilistic analysis to quantify the impact of manufacturing variability on the liner low-cycle fatigue life for two gas turbine combustors. The probabilistic analysis showed that liner temperature variability reduces the typical combustor life by approximately 20 percent of the nominal life for the combustors studied, and that the probability that a randomly selected combustor will fail earlier predicted using deterministic methods is approximately 80 percent. The probabilistic analysis also showed that the material property variability accounts for approximately 80 percent of the variability exhibited in the field failure data.

- Application of a sensitivity analysis to identify the leading drivers of combustor liner low-cycle fatigue life. The variability of the combustor mixedness and the material property variability are found to be the leading drivers of the typical combustor life and the minimum combustor life, respectively. Decreasing the variability of these quantities are shown to decrease the likelihood that combustor liners will fail earlier than predicted using deterministic methods.

Chapter 2

Combustor Modeling

2.1 Introduction

This chapter presents a simplified combustor model that establishes causal relationships amongst geometric design parameters, material properties, liner temperature, and liner life. The model consists of several elements: a network flow analysis, a combustor temperature field analysis, a liner heat transfer analysis, and a low-cycle fatigue life analysis. These elements are shown in Figure 2.1. The model inputs are the mean values and standard deviations of random variables representing the effects of manufacturing variability. The outputs are the liner temperatures and the liner low-cycle fatigue life. The mean and standard deviation of the random inputs are determined from geometric design specifications, manufacturing tolerances, data scatter about a response surface for the crack-initiation life, and a statistical assessment of the near-wall gas temperature variability at the combustor outlet. The outputs are assessed using combustor wall temperatures measurements and field failure data obtained from an engine company. The input and output parameters used in the combustor model are shown in Tables 2.1, 2.2, and 2.3. The physical principles, combustor rig data, and numerical data used to determine the values of these parameters are also indicated in the tables.

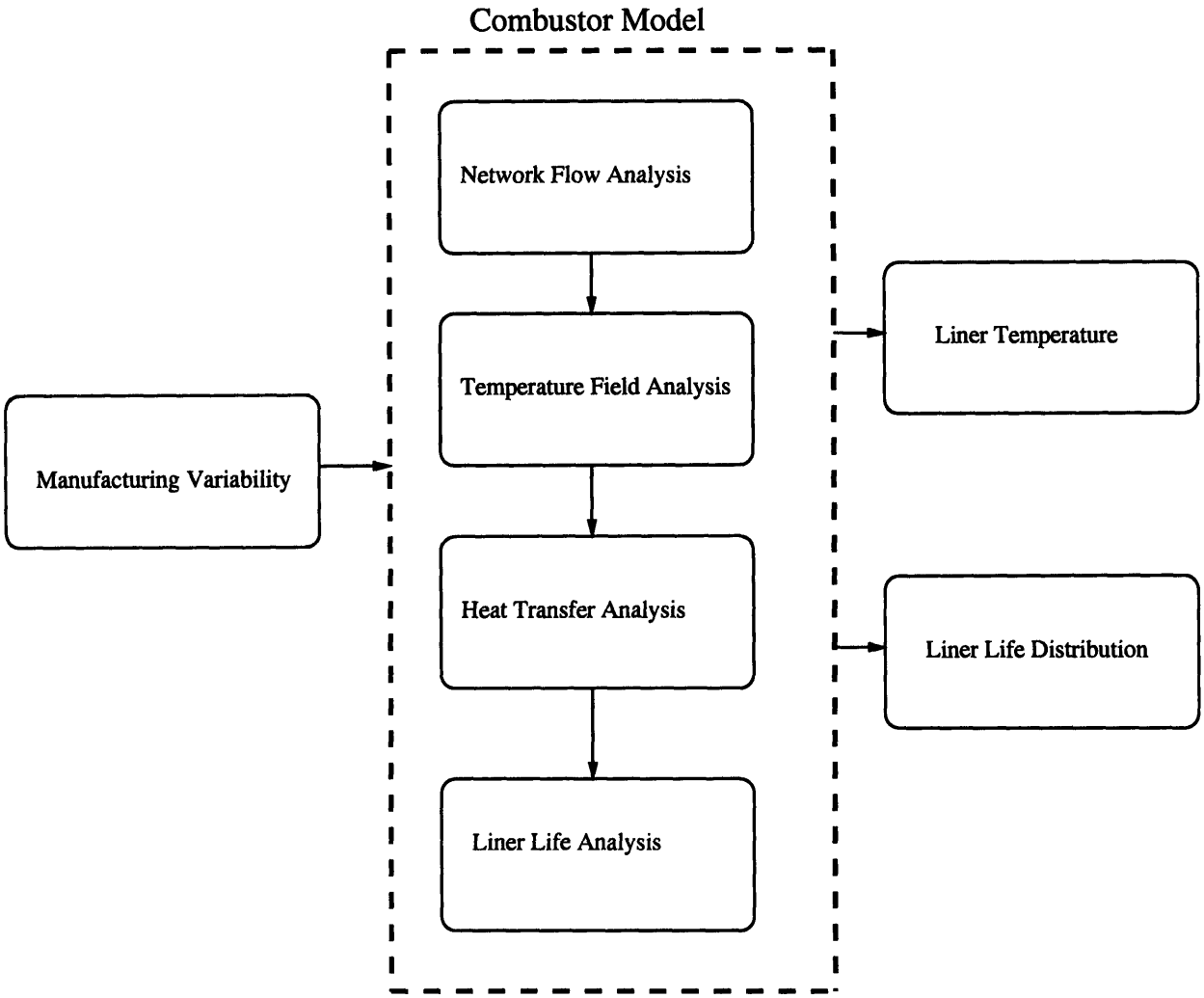

Figure 2-1: Probabilistic modeling framework for assessing the impact of manufacturing variability on combustor liner temperature and liner life.

Table 2.1: Random Input Variables

Quantity	Calculated/obtained from	Physical principle/data used
Hole size multiplier (δ_d)	Engine company	Cooling hole tolerances
Slot height (s)	Engine company	Geometric tolerance
TBC emissivity (ϵ_{tbc})	Engine company	TBC specification
TBC thickness (t_{tbc})	Engine company	Spray process capability
Bond coat thickness (t_{bnd})	Engine company	Process capability
Liner thickness (t_m)	Engine company	Geometric tolerance
TBC thermal conductivity (k_{tbc})	Engine company	Material property data
Liner thermal conductivity (k_m)	Engine company	Material property data
Bond coat thermal conductivity (k_{bnd})	Engine company	Material property data
Dome air flow conductance (G_{air})	Engine company	Combustor rig data
Fuel mass flow rate ($\dot{m}_{fuel}$)	Engine company	Fuel flow curves/limits
Combustor mixedness parameter (ζ)	Engine company	Outlet temperature data
Material property variability of life curve (Ψ)	Engine company	Data scatter (LCF life curve)

Table 2.2: Random Output Variables

Quantity	Calculated/obtained from	Physical principle/data used
Liner life (N_f)	Probabilistic model	LCF life analysis
Liner temperature (T_{mh})	Probabilistic model	Heat transfer analysis

Table 2.3: Deterministic Input Parameters

Quantity	Calculated/obtained from	Physical principle/data used
Burner length (L_c)	Engine company	Part drawing
Compressor discharge density (P_3)	Engine company	Cycle requirement
Compressor discharge temperature (T_3)	Engine company	Cycle requirement
Stoichiometric fuel-air ratio (f_{st})	Calculated	Stoichiometry
Velocity profile factor (PF_v)	Engine company	FLUENT
Stefan-Boltzmann constant ($\bar{\sigma}$)	Literature	Physical constant
Burner area (A_b)	Engine company	Combustor dimensions
Baseline stress ($\hat{\sigma}_{base}$)	Engine company	ANSYS
Baseline liner temperature (T_{mh})	Engine company	ANSYS
Flame luminosity ($\hat{L}$)	Literature	Correlation
Mean beam length (l_b)	Calculated	Radiation transfer theory

The simplified model was applied to two combustors used on commercial aircraft engines, referred to as combustors A and B. These combustors contain I liner panels and J annular sectors, or cup sections, as shown in Figures 2-2 and 2-3, respectively. The walls of these combustors are convectively cooled by a combination of film cooling on the flame side and by the bypass air on the cold side. The primary failure mode of these combustor liners is thermo-mechanical fatigue which arises due to thermal straining of the liner between the start-up and shutdown of the engine [33]. These thermal strains are caused by elevated liner temperatures and temperature gradients [15].

Combustors A and B differ in many ways. Notably, they are from two different engine families with different cycle conditions. These conditions result in different combustor outlet temperatures. Moreover, the nominal air flow distributions around the liners of combustor A and B yield different bulk gas temperatures, liner temperatures, and liner lives. Finally, combustor B has been in the field for a longer period of time than combustor A and has a long record of unscheduled removals due to combustor liner distress while combustor A has not caused any such events to date [34].

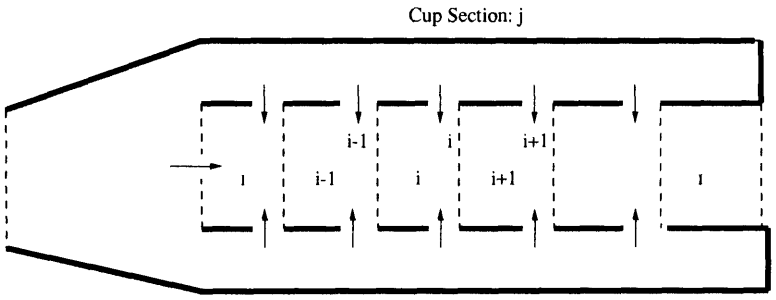

Figure 2-2: Sketch of a combustor with I panels.

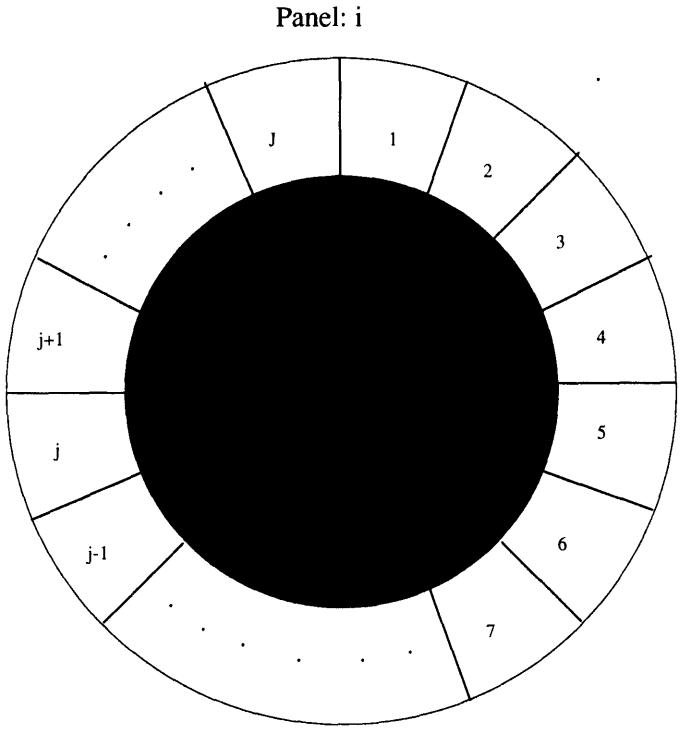

Figure 2-3: Sketch of a combustor with J sectors, or cup sections.

2.2 Network Flow Analysis

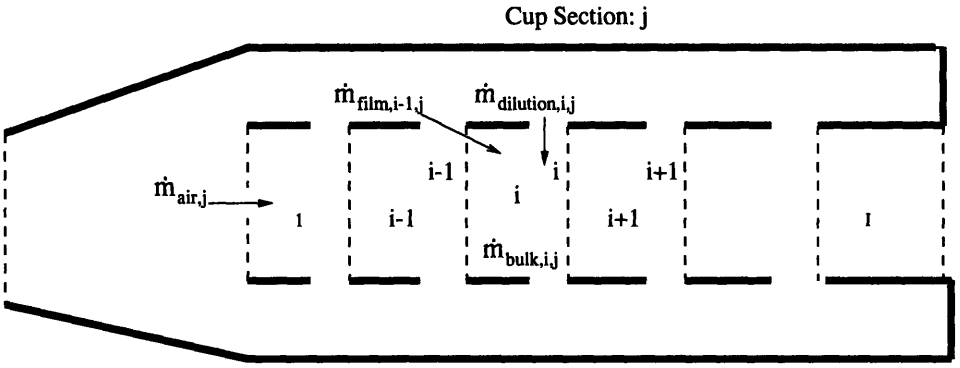

Figure 2-4: Sketch of the mass flows crossing the combustor liner.

Application of a network flow analysis to gas turbine combustors links the mass flows across the liner and the bulk gas mass flows inside the liner. The bulk gas mass flows are related by

$$\dot{m}_{bulk,i,j} = \dot{m}_{bulk,i-1,j} + \dot{m}_{film,i-1,j} + \dot{m}_{dilution,i,j}, \tag{2.1}$$

where $\dot{m}_{bulk,i,j}$, $\dot{m}_{film,i,j}$, and $\dot{m}_{dilution,i,j}$ are the bulk gas mass flow, the film cooling mass flow, and the dilution air mass flow, respectively, for the i^{th} panel and j^{th} cup section, as shown in Figure 2-4. The bulk mass flow that crosses the i^{th} face of cell i ($\dot{m}_{bulk,i,j}$) is equal to the sum of the bulk mass flow that crosses the $i-1$ face of the i^{th} cell ($\dot{m}_{bulk,i-1,j}$), the dilution air that enters the i^{th} cell ($\dot{m}_{dilution,i,j}$), and the film cooling air that enters the $i-1$ cell ($\dot{m}_{film,i-1,j}$). The total combustor mass flow and the mass flows crossing the liner are related by the following equation to satisfy the conservation of mass,

$$\dot{m}_c = \sum_{j=1}^{J} \dot{m}_{air,j} + \sum_{i=1}^{I-1}\sum_{j=1}^{J} \dot{m}_{film,i,j} + \sum_{i=1}^{I-1}\sum_{j=1}^{J} \dot{m}_{dilution,i,j}, \tag{2.2}$$

where $\dot{m}_c$ is the total combustor mass flow, $\dot{m}_{air,j}$ is the mass flow across the dome, $\dot{m}_{film,i,j}$ is the cooling film mass flow, and $\dot{m}_{dilution,i,j}$ is the dilution air mass flow. The dome, film, and dilution mass flows are estimated using Equations 2.3, 2.4, and 2.5, respectively,

$$\dot{m}_{air,j} = G_{air,j}\sqrt{2\rho_3(P_3 - P_4)} \tag{2.3}$$

$$\dot{m}_{film,i,j} = G_{film,i,j}\sqrt{2\rho_3(P_3 - P_4)} \tag{2.4}$$

$$\dot{m}_{dilution,i,j} = G_{dilution,i,j}\sqrt{2\rho_3(P_3 - P_4)}, \tag{2.5}$$

where $G_{air,j}$ is the mass flow conductance across the dome, $G_{film,i,j}$ is the mass flow conductance for the film, $G_{dilution,i,j}$ is the mass flow conductance for the dilution air, ρ_3 is the density of the compressor discharge air, P_3 is the pressure of the compressor discharge air, and P_4 is the pressure of the combustor discharge flow.

In the probabilistic analysis, the mass-flow conductances and the combustor discharge pressure will vary. The probabilistic analysis assumes that the combustor mass flow, $\dot{m}_c$, is the same from combustor to combustor. Furthermore, the analysis assumes that the combustor pressure is uniform throughout a given combustor. Then, in the probabilistic analysis, for a given set of mass-flow conductances and P_3, the local film, dilution, and bulk mass flows can be found by solving Equations 2.3, 2.4, and 2.5. This solution is readily found using a standard circuit analogy since the combustor flow network is equivalent to a parallel resistance network.

The nominal mass flow conductances were determined from rig test data provided by an engine company [19]. Specifically, the mass flow data for each air admission port were applied to estimate the corresponding nominal flow conductances using

$$G^{nom}_{X,i,j} = \frac{\dot{m}^o_{X,i,j}}{\sqrt{2\rho^o_3(P^o_3 - P^o_4)}}, \tag{2.6}$$

where $G^{nom}_{X,i,j}$ is the nominal conductance of flow type X, $\dot{m}^o_{X,i,j}$ is the mass flow for flow type X, P^o_3 is the compressor discharge pressure, and P^o_4 is the combustor discharge pressure. The superscript, o, indicates that the parameter value was obtained from combustor rig data. The standard deviation of $G_{air,j}$ was estimated from mass-flow tolerance limits specified by an engine company [34]. The variability of the conductances for the film- and dilution-flows were determined from

$$\frac{G_{film,i,j}}{G^o_{film,i,j}} = \delta^2_{d,i,j} \tag{2.7}$$

and

$$\frac{G_{dilution,i,j}}{G^o_{dilution,i,j}} = \delta^2_{d,i,j}, \tag{2.8}$$

where $\delta_{d,i,j}$ is a parameter that represents the variability of the film hole and the dilution hole diameters. $\delta_{d,i,j}$ is a normally-distributed random variable with unity mean and a standard deviation based on the tolerances of the cooling holes. The mass flow conductances are linearly related to the cooling hole areas, and, in turn, quadratically related to the cooling hole diameters.

The fuel injector mass flow for the j^{th} cup section, $\dot{m}_{fuel,j}$, is determined from a curve relating the fuel flow to the injector pressure drop [34]. The fuel injector mass flow and the air mass flow distributions yield the bulk flow equivalence ratio distribution in the combustor, as shown in Equation 2.9,

$$\phi_{i,j} = (\frac{1}{f_{st}})(\frac{\dot{m}_{fuel,j}}{\dot{m}_{bulk,i,j}}), \tag{2.9}$$

where $\phi_{i,j}$ is the equivalence ratio for the i^{th} cell and the j^{th} cup section, and f_{st} is the stoichiometric fuel-to-air ratio.

As described in this section, the probabilistic network flow analysis has employed several assumptions. In summary, these assumptions are:

1. **The total mass flow rate is the same for all combustors.** All combustors pass the same mass flow without regard for the variability of the mass flow conductances. Total temperature variability and total pressure variability yield mass flow variability

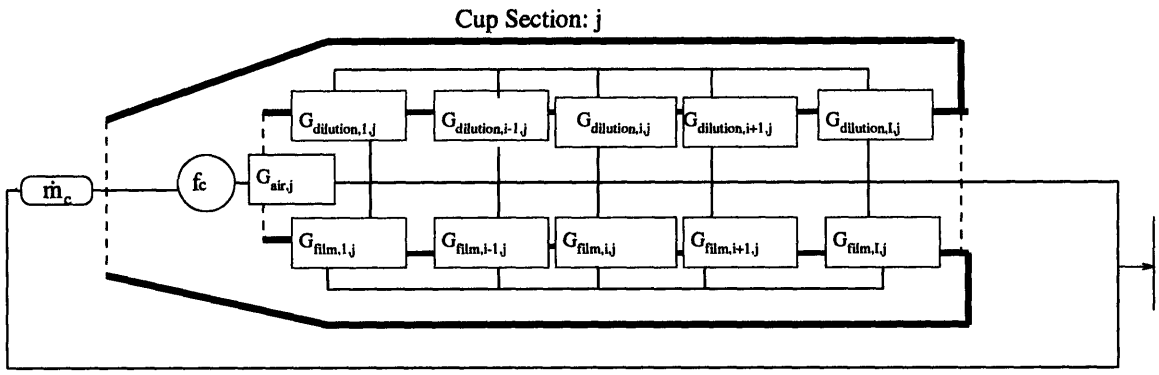

Figure 2-5: Sketch of the combustor mass flow circuit. $\dot{m}_c$ is the total combustor mass flow, $G_{film,i,j}$ is the flow conductance for the film flow, $G_{dilution,i,j}$ is the flow conductance for the dilution mass flow, $G_{air,j}$ is the conductance for the dome flow, and f_c is the mass flow-pressure drop function.

for a choked turbine nozzle. This implies that the outlet temperature variability, outlet total pressure variability, and the bulk mass flow variability are coupled. The network model does not account for this effect.

2. **The flow across the combustor liner is incompressible.** The low pressure drop across the liner yields low Mach Number flow. For adiabatic, low Mach number flows without heat release due to chemical reactions, density changes are negligible.

3. **The combustor pressure is uniform.** A uniform combustor pressure facilitates the application of the circuit model to estimate the combustor mass flow splits. Although there are static pressure gradients inside the combustor, the magnitude of these gradients are less than 20 percent of the overall liner pressure drop. Application of this assumption in model yields one value of the mass flow-pressure drop function for branches of the circuit for each combustor.

4. **There is no mixing in the circumferential direction between adjacent cup section flows.** This assumption was made in order to treat each cup section independently of the other cup sections.

5. **The dilution air mixes instantaneously with the bulk flow over each panel.** The dilution air is typically injected at 90 degrees to the liner surface. The dilution jet mixes directly with the combustion products and, ultimately, decreases the bulk gas equivalence ratio. It is assumed that this process occurs instantaneously in the model due to the high mixing rates promoted by elevated turbulence levels of combustor flows.

6. **The cooling film flow mixes with bulk flow in the adjacent downstream panel.** The cooling film is injected tangentially along the liner surface and is nearly-degraded at the end of the panel. It is assumed that this cooling flow does not mix with the adjacent combustion products. As a result, the bulk gas equivalence ratio is unaffected by the presence of the cooling film.

7. **The fuel injector mass flow rate has a negligible impact on the combustor flow splits.** The fuel flow is approximately three percent of the overall air mass flow for most combustor combustors.

2.3 Temperature Field Analysis

A lumped-parameter analysis is used to determine the combustion gas temperatures and the film temperature. The combustor temperature field adjacent to each panel is divided into three elements: the bulk gas temperature, the near-wall gas temperature, and the cooling film temperature. An illustration of these elements is shown in Figure 2-6. A detailed description of the lumped-parameter analysis is presented in this section.

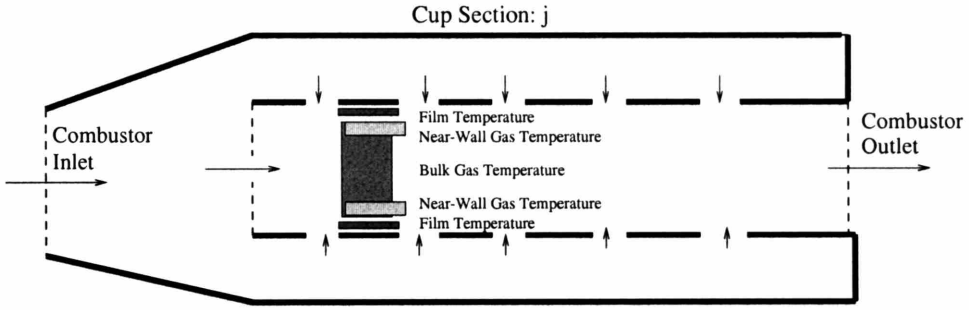

Figure 2-6: Sketch of a lumped-parameter model for the combustor temperature field. The temperature field is separated into three driving temperatures and applied in a one-dimensional heat transfer analysis. These temperatures are the bulk gas temperature, the near-wall gas temperature, and the cooling film temperature.

2.3.1 Bulk Gas Temperature

The bulk gas temperature ($T_{bulk,i,j}$), the temperature of the mainstream flow near i^{th} panel and j^{th} cup section, is computed using a response surface equation relating the bulk gas temperature to the compressor discharge temperature (T_3) and the bulk gas equivalence ratio ($\phi_{i,j}$), as shown in

$$T_{bulk,i,j} = g_1(T_3, \phi_{i,j}). \tag{2.10}$$

The response surface equation was created by performing a well-stirred reactor analysis at the combustor pressure and average residence time over a range of T_3 and ϕ and, then, applying a regression analysis to these data. The details of the well-stirred reactor analysis and the response surface analysis are presented below.

Well-Stirred Reactors

Well-stirred reactors (WSR) are idealized open flow systems in which the combustion products are perfectly mixed with the incoming reactants. The mass fractions and the temperatures of the mixtures inside the reactor are the same as those at the outlet. This homogeneity is promoted by fast, turbulent mixing levels. WSRs are used to investigate

ignition characteristics of many open flow combustion systems [36]. For example, the turbulent combustion in the recirculation zones formed by bluff bodies in diffusion and premixed flames.

The assumptions for a steady-state, well-stirred reactor analysis are:

1. The reacting mixture is perfectly mixed inside the combustion chamber.
2. The ratio of the mixing time to the chemical ignition time is much less than one.
3. The ratio of heat losses to the enthalpy rise is small; the combustion process is adiabatic.
4. The thermodynamic states of the combustion products at the outlet and inside the combustion chamber are the same.
5. The pressure is uniform inside the combustion chamber.
6. The reactor is in steady-state.

Jet fuel is composed of approximately 1000 hydrocarbons and simulating the chemical reactions of all of these species is computationally expensive. A reduced chemical kinetic mechanism with 13 species and 20 reactions steps to determined the temperature and composition of the combustion products[41]. This chemical kinetic mechanism is presented in Appendix C.

The species and energy conservation equations,

$$\frac{1}{\tau_{res}}(Y_k - Y_{k,0}) = \frac{\omega_k}{\rho_{bulk}} \tag{2.11}$$

$$\frac{1}{\tau_{res}}\sum_{k=1}^{K} Y_k(h_k - h_{k,0}) = \sum \frac{h_k \omega_k}{\rho_{bulk}}, \tag{2.12}$$

are solved in CHEMKIN III to determine the chemical composition and temperature of the combustion products [17]. In Equations 2.11 and 2.12, ρ_{bulk} is the mixture density, ω_k is the reaction rate of species k, Y_k is the mass fraction of species of chemical species k at the inlet, and $Y_{k,0}$ is the mass fraction of chemical species k at the outlet, h_k is the specific enthalpy of species k at the outlet, and $h_{k,0}$ is the specific enthalpy of species k at the inlet, and τ_{res} is the reactor residence time. τ_{res} is determined from

$$\tau_{res} = \frac{\rho_{bulk} V}{\dot{m}_{bulk}}, \tag{2.13}$$

where $\dot{m}_{bulk}$ is the mass flow rate inside the reactor, and V is the reactor volume. The mixture density is determined from

$$\rho_{bulk} = \frac{P_4}{R_{gas} T_{bulk}}, \tag{2.14}$$

where R_{gas} is the gas constant for the combustion products, and T_{bulk} is the bulk gas temperature of the combustion products. The specific enthalpy of species k, h_k, is determined from

$$h_k = h^o_{f,k} + \int_{T_o}^{T} C_{p,k} dT, \tag{2.15}$$

where $h^o_{f,k}$ is the enthalpy of formation of species k, $C_{p,k}$ is the specific heat at constant pressure of species k, and T_o is a reference temperature. T_o is 298.15 degrees Kelvin.

Well-Stirred Reactor Analysis

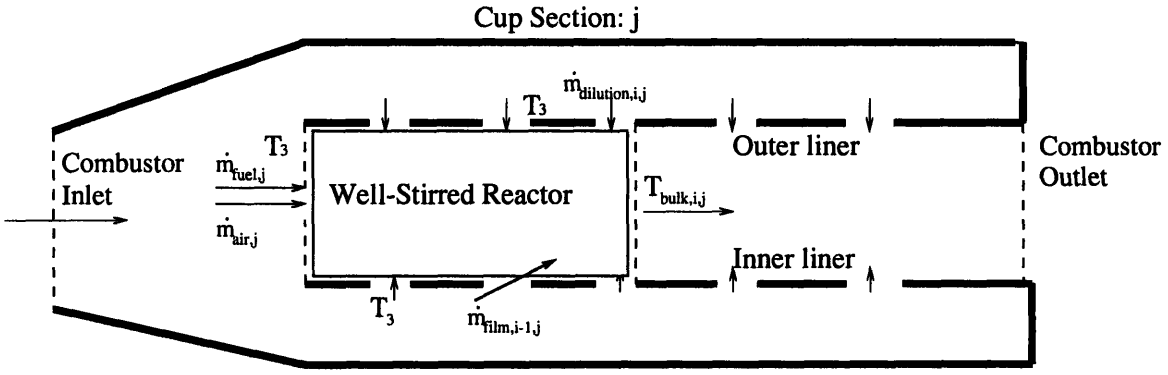

Figure 2-7: Application of a well-stirred reactor analysis to estimate of the bulk gas temperature in the i^{th} panel and j^{th} cup section. The reactor inlets consist of the air admission ports at the dome, the outer liner, and the inner liner. The reactor outlet faces the combustor outlet.

A well-stirred reactor, shown in Figure 2-7, was applied to estimate the bulk gas temperature for the i^{th} panel and j^{th} cup section as a function of the bulk equivalence ratio and the compressor discharge air temperature. The reactor inlets consist of the air admission ports at the dome, the outer liner, and the inner liner. The inlet temperature of the WSR is T_3. The fuel and air that cross the dome, the inner liner, and the outer liner are used to estimate the equivalence ratio. The bulk mass flow inside the reactor is determined from

$$\dot{m}_{bulk,i,j} = \dot{m}_{air,j} + \sum_{1}^{i-1} \dot{m}_{film,i,j} + \sum_{1}^{i} \dot{m}_{dilution,i,j}. \tag{2.16}$$

The bulk gas temperature is calculated by performing a WSR calculation with the estimated equivalence ratio and T_3.

Surrogate Model

A surrogate model for the bulk gas temperature was created to decrease the computation time during the probabilistic analysis. A well-stirred reactor analysis was performed for a range of values for T_3 and ϕ while the combustor pressure and average residence time were held constant. The data points for T_3 were between 700 K and 850 K in 25 K increments, and the ϕ data points ranged from 0.4 to 1.8 in increments of 0.1. These data points represent the range of equivalence ratios and compressor discharge temperatures characteristic of combustors A and B. The flame temperature estimates were fitted to a fourth-order polynomial function of ϕ. The regressors of this polynomial were then fitted to fourth-order

polynomial in T_3 by performing a second regression analysis. Surrogate model for the bulk gas temperature is

$$T_{bulk} = g_1(T_3, \phi) = \sum_{n=0}^{4} a_n(T_3)\phi^n, \tag{2.17}$$

where the regression coefficients, a_i, are functions of T_3. The compressor discharge temperature, as shown in

$$\hat{T}_3 = \frac{T_3 - \mu_{T3}}{\sigma_{T3}}, \tag{2.18}$$

is normalized by subtracting the mean value (μ_{T_3}) and dividing by the standard deviation (σ_{T3}) for a range of T_3 data points. Each regression coefficient is a fourth-order polynomial function of $\hat{T}_3$, as shown in

$$a_0 = \alpha_{0,0} + \alpha_{0,1}\hat{T}_3 + \alpha_{0,2}\hat{T}_3^2 + \alpha_{0,3}\hat{T}_3^3 + \alpha_{0,4}\hat{T}_3^4 \tag{2.19}$$

$$a_1 = \alpha_{1,0} + \alpha_{1,1}\hat{T}_3 + \alpha_{1,2}\hat{T}_3^2 + \alpha_{1,3}\hat{T}_3^3 + \alpha_{1,4}\hat{T}_3^4 \tag{2.20}$$

$$a_2 = \alpha_{2,0} + \alpha_{2,1}\hat{T}_3 + \alpha_{2,2}\hat{T}_3^2 + \alpha_{2,3}\hat{T}_3^3 + \alpha_{2,4}\hat{T}_3^4 \tag{2.21}$$

$$a_3 = \alpha_{3,0} + \alpha_{3,1}\hat{T}_3 + \alpha_{3,2}\hat{T}_3^2 + \alpha_{3,3}\hat{T}_3^3 + \alpha_{3,4}\hat{T}_3^4 \tag{2.22}$$

$$a_4 = \alpha_{4,0} + \alpha_{4,1}\hat{T}_3 + \alpha_{4,2}\hat{T}_3^2 + \alpha_{4,3}\hat{T}_3^3 + \alpha_{4,4}\hat{T}_3^4. \tag{2.23}$$

A comparison of the estimation error of the bulk gas temperature surrogate model to the CHEMKIN estimate is shown in Figure 2-8. The estimation error is less than one percent of the CHEMKIN estimate for the range of equivalence ratios and compressor discharge temperatures characteristic of combustors A and B. This error is less than the level of uncertainty of using a surrogate fuel to estimate temperature of the combustion products.

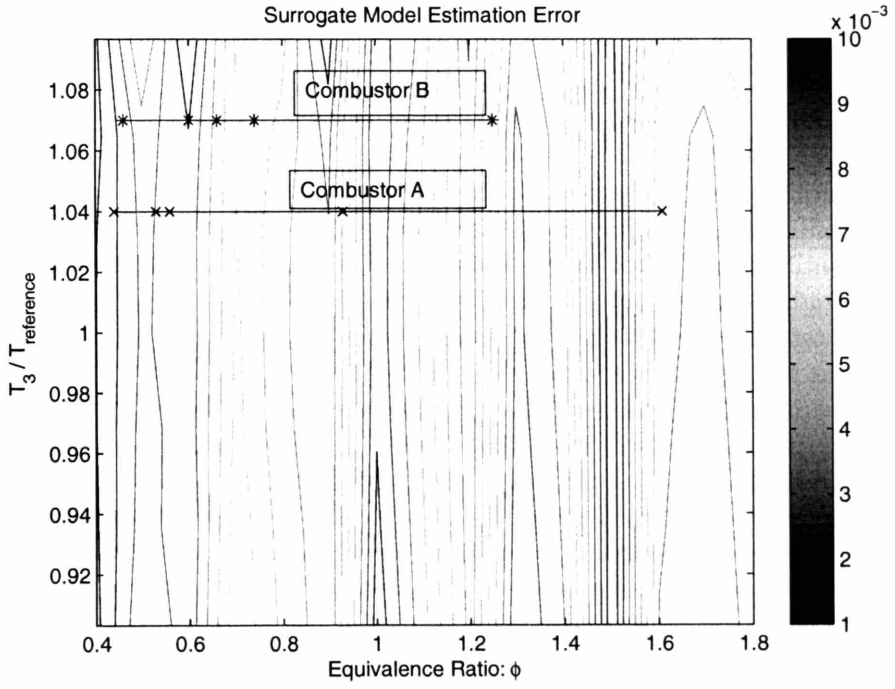

Figure 2-8: Contour plot of the estimation error of the surrogate model. The ordinate is the compressor discharge temperature divided by a reference temperature. The abscissa is the bulk gas equivalence ratio. The error is determined by taking difference between the response surface estimate and the CHEMKIN estimate, dividing the difference by the CHEMKIN estimate, and then taking the absolute value of the quotient. The nominal equivalence ratios for combustors A and B are shown in the contour plot.

2.3.2 Near-Wall Gas Temperature

The near-wall gas temperature ($T_{gas,i,j}$) is the temperature of the flow near the liner wall and above the cooling film for the i^{th} panel and j^{th} cup section. The difference between bulk gas temperature and the near-wall gas temperature is an indication of the radial inhomogeneity of the combustor temperature field. Fast mixing promoted by elevated turbulence levels in the combustion chamber increases the homogeneity of the temperature field. A first-principles approach that links the effects of manufacturing variability to the radial temperature gradients could not be obtained due to the complexity of the combustor aerodynamics and chemistry. As a result, an empirical model was applied in the probabilistic analysis to account for the magnitude and the variability of these radial gas temperature gradients. The empirical model is

$$\frac{T_{gas,i,j} - T_3}{T_{bulk,i,j} - T_3} = g_2(\zeta_{i,j}, \frac{x_c}{L_c}) = 1 - e^{(-\zeta_{i,j}\frac{x_c}{L_c})}, \tag{2.24}$$

where x_c is the longitudinal distance from the fuel injector, L_c is the combustor length, and g_2 is a function for the radial gas temperature gradient. $\zeta_{i,j}$, an empirically-determined parameter, quantifies the impact of the complex turbulent mixing processes inside the combustor on the radial gas temperature profiles near each liner panel. Higher values of $\zeta_{i,j}$ result in flatter temperature profiles than lower values. In particular, the difference between the near-wall gas temperatures and the bulk gas temperatures decrease exponentially as the combustor mixedness level and the distance from the front of the combustor increase. g_2, which is equal to zero at the front of the combustor, signifies that the near-wall gas temperature is equal to the film cooling air temperature. The nominal value of g_2 was determined using rig data for the outlet temperature field, where the bulk temperature is defined as the raw average of the outlet temperature measurements in each cup section, and the outlet near-wall gas temperature is defined as the raw average of the thermocouple measurements adjacent to the liner wall in each cup section.

2.3.3 Film Temperature

The film cooling flow impacts the liner convection heat transfer load by altering the near-wall film temperature and velocity profiles [1]. The film effectiveness, η, models the effects of the former. This parameter is used to calculate the cooling film temperature, T_{film}, along the combustor liner. The film effectiveness is related to the film temperature, the near-wall gas temperature, and the compressor discharge air temperature for the i^{th} panel and j^{th} cup section by

$$\eta_{i,j} = \frac{T_{gas,i,j} - T_{film,i,j}}{T_{gas,i,j} - T_3}. \tag{2.25}$$

The film effectiveness parameter correlation is a function of the distance from the cooling slot, the cooling slot height (s), and the blowing parameter (B) [1]. The film effectiveness is applied to the degraded cooling film for one panel length for combustors A and B. The heat flux scales with the cooling film mass flow over the liner surface [37]. The blowing parameter, a non-dimensional measure of the mass flux of the cooling film, captures this effect. B is defined as the ratio of the cooling film mass flux to the mass flux of the near-wall gas flow, as shown in

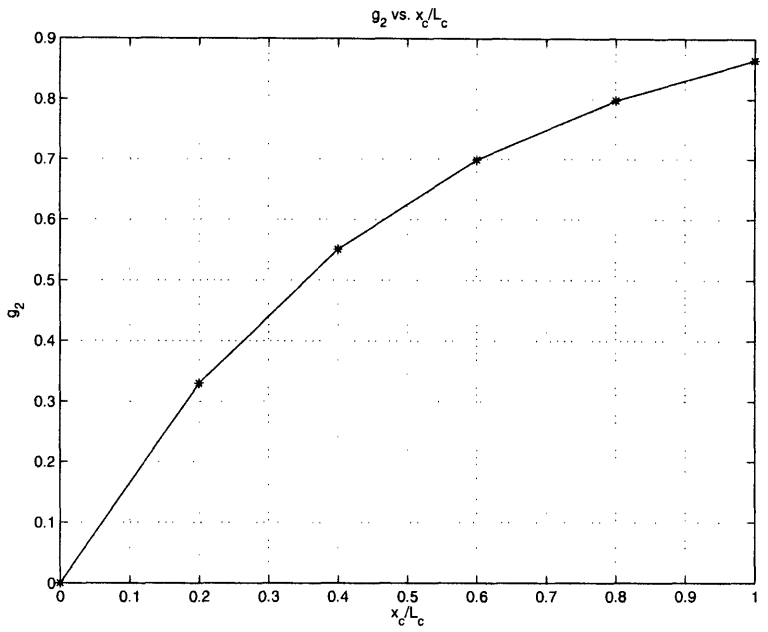

Figure 2-9: Influence of mixedness parameter on radial temperature gradients by panel. g_2 is plotted vs. x_c/L_c for $\zeta_{i,j} = 2.0$.

$$B_{i,j} = \frac{(\frac{\dot{m}_{film,i,j}}{A_{s,i,j}})}{(\frac{\dot{m}_{bulk,i,j}}{A_{b,i,j}})} \frac{1}{PF_{v,i}}, \tag{2.26}$$

where $\dot{m}_{film,i,j}$ is the film mass flow, $A_{s,i,j}$ is the slot area, $\dot{m}_{bulk,i,j}$ is the bulk mass flow, $A_{b,i,j}$ is the combustor flow path area, and $PF_{v,i}$, the velocity profile factor, is the ratio of the near-wall combustion gas flow velocity to the average combustion gas flow velocity. The value of $PF_{v,i}$ are determined from the available CFD data of the combustor velocity field [19]. The slot area ($A_{s,i,j}$) is given by

$$A_{s,i,j} = 2\pi R_s s_{i,j}, \tag{2.27}$$

where $s_{i,j}$ is the slot height, and $R_{s,i}$ is the radius of the cooling slot from the combustor centerline. $R_{s,i}$ is larger for the outer liner than for the inner liner at the i^{th} panel. Combining Equations 2.25, 2.26, and 2.27 yields

$$\frac{T_{gas,i,j} - T_{film,i,j}}{T_{gas,i,j} - T_3} = g_3(\delta_{d,i,j}, s_{i,j}, \dot{m}_{air,i,j}), \tag{2.28}$$

which is a function of three randomly varying parameters: $\delta_{d,i,j}$, $s_{i,j}$, and $\dot{m}_{air,i,j}$.

2.3.4 Deterministic Analysis

The results of a deterministic analysis of these elements are shown in Figure 2-10. The bulk temperatures are greater than the near-wall temperatures in the model. Furthermore, the film temperature is lower than the bulk and near-wall gas temperatures. The difference

between bulk gas temperature and the near-wall gas temperature decreases as the distance from the front of the combustor increases. This simulates the increased homogeneity of the flow along the main gas path due to turbulent mixing.

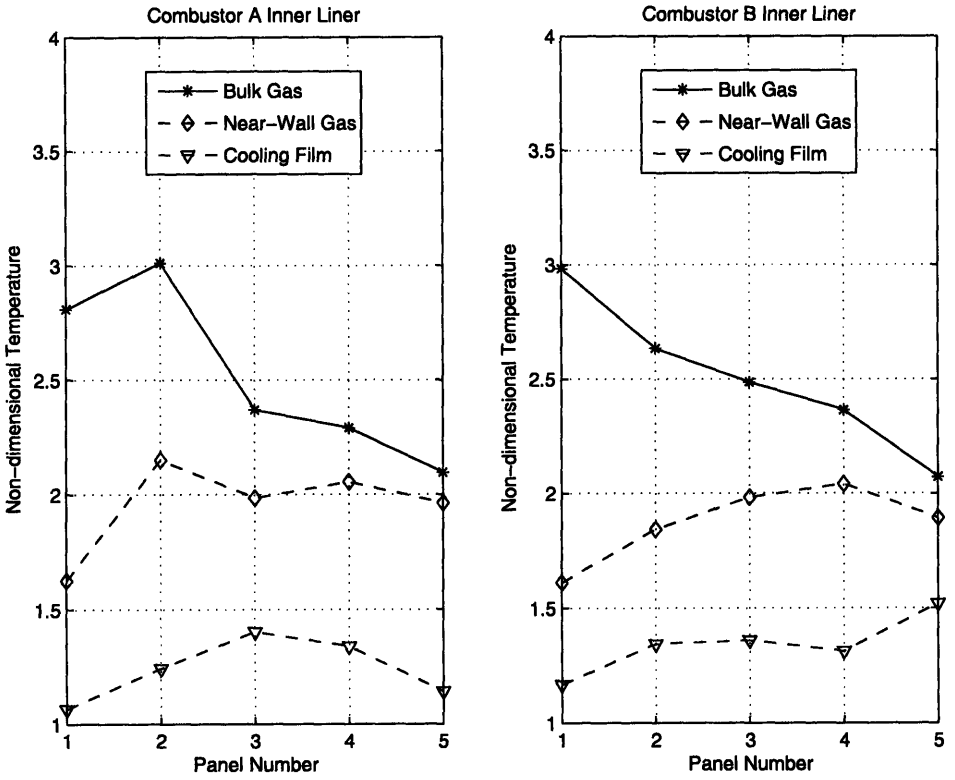

Figure 2-10: Lumped-parameter analysis of combustor temperature field for combustors A and B. The gas temperature normalized by the compressor discharge air temperature vs. the panel number is plotted in this figure.

2.4 Heat Transfer Analysis

A steady, one-dimensional heat transfer analysis is performed to estimate the hot-side metal temperature on the inner and outer liner in the i^{th} panel and j^{th} cup section. The model incorporates the effects of radiation, convection, and conduction, as shown in

$$\dot{q}_{i,j} = h_{f,i,j}(T_{film,i,j} - T_{tbc,i,j}) + \frac{1}{2}(1+\epsilon_{tbc})\bar{\sigma}(\epsilon_{rad,i,j}{T_{rad,i,j}}^4 - \alpha_{rad,i,j}{T_{tbc,i,j}}^4) \tag{2.29}$$

$$\dot{q}_{i,j} = \frac{k_{tbc}}{t_{tbc}}(T_{tbc,i,j} - T_{bnd,i,j}) \tag{2.30}$$

$$\dot{q}_{i,j} = \frac{k_{bnd}}{t_{bnd}}(T_{bnd,i,j} - T_{mh,i,j}) \tag{2.31}$$

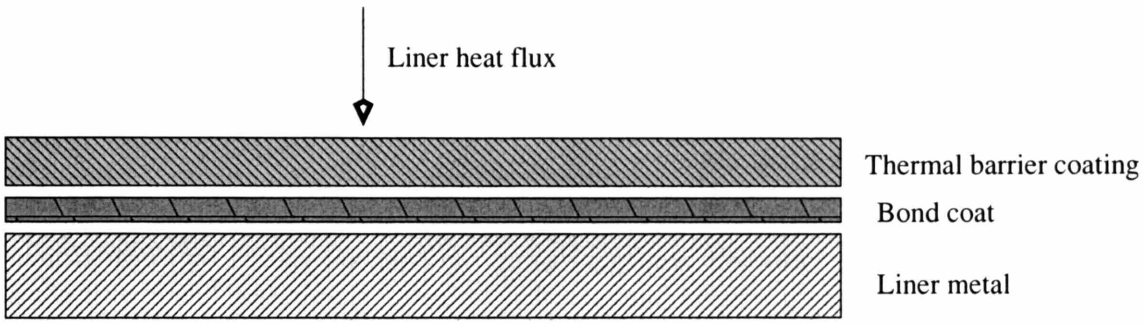

Figure 2-11: Sketch of a combustor liner wall.

$$\dot{q}_{i,j} = \frac{k_m}{t_m}(T_{mh,i,j} - T_{mc,i,j}) \tag{2.32}$$

$$\dot{q}_{i,j} = h_{b,i,j}(T_{mc,i,j} - T_3) \tag{2.33}$$

$$\frac{\alpha_{rad,i,j}}{\varepsilon_{rad,i,j}} = \left(\frac{T_{rad,i,j}}{T_{tbc,i,j}}\right)^{1.5} \tag{2.34}$$

$$\varepsilon_{rad,i,j} = 1 - \exp(-28600 P_4 \hat{L}(f_{st}\phi_{i,j} l_b)^{0.5}(T_{rad,i,j})^{-1.5}). \tag{2.35}$$

The random inputs are the thermal conductivities and thicknesses of the TBC, bond coat, and liner (k_{tbc}, k_{bnd}, k_m, t_{tbc}, t_{bnd}, t_m) and the TBC surface emissivity (ϵ_{tbc}). The random output is the hot-side metal temperature (T_{mh}). The effective radiation temperature ($T_{rad,i,j}$) is set equal to the bulk gas temperature ($T_{bulk,i,j}$). The liner heat flux ($\dot{q}$) and the TBC, bond coat, and liner temperatures (T_{tbc}, T_{bnd}, T_{mh}, T_{mc}) are estimated by solving the model equations with a Newton-Raphson method.

Several simplifying assumptions were made in order to perform the heat transfer analysis. The convection heat transfer coefficient on the hot side ($h_{f,i,j}$) is determined from a correlation for turbulent flow over a flat plate [20], and the backside heat transfer coefficient ($h_{b,i,j}$) is estimated from a correlation for thermally developing flow through a long, concentric duct [21]. The combustor pressure (P_4) is assumed to be spatially uniform, consistent with the assumption made in the network flow model. It is assumed that there is a radiative exchange between a nongray, isothermal gas and a single-surface gray enclosure located at the mean beam length (l_b) [28].

The primary zone contains soot particles that radiate thermal energy in the infrared part of the electromagnetic spectrum [1]. These particles radiate as blackbodies. As a result, they increase the radiative loads to the liner panel that surrounds the primary zone. The flame luminosity factor ($\hat{L}$) accounts for these effects by increasing the magnitude of the combustion gas emissivity estimate. There are several correlations for the flame luminosity factor. Most correlations relate the flame luminosity to the carbon-to-hydrogen ratio of the fuel. Lefebvre's correlation [44], which relates the flame luminosity to the hydrogen content of the fuel, is used in this thesis. The soot concentration decreases downstream of the primary zone. As a result, the flame luminosity factor would decrease accordingly [43]. In order to simplify the modeling of the radiative heat transfer process inside the combustor

while accurately estimating the radiative loads, it is assumed that the combustion gas is luminous near panel one and nonluminous elsewhere.

2.5 Liner Life Analysis

The primary failure mode for the combustor liners studied is low-cycle fatigue (LCF) [32, 33, 34]. The cracks that form and propagate along the liner are caused by elevated liner temperatures, temperature gradients, and thermal stresses. Combustor liners with crack lengths exceeding specified limits are classified as failed parts. The model output is the low-cycle fatigue life. The random input to the life model is the hot-side liner temperature, and the deterministic inputs are compressor discharge temperature, the baseline liner stress, the baseline liner temperature, and a parameter that accounts for the material property variability.

An LCF life analysis was applied to each section of the combustor liner in order to account for these effects. For a combustor with J cup sections, I panels, an inner liner, and an outer liner, the number of liner life calculations equals $2IJ$. The overall liner life for each combustor is defined as the minimum life in a set consisting of $2IJ$ points. The failure of one part of the liner constitutes an overall failure for the combustor.

2.5.1 Crack Initiation Life

The crack initiation life analysis was based on a low-fidelity model used by an engine company [32]. The model consists of two curves: an average life curve and a minimum life curve. The curves are sketched in Figure 2-12. The average life curve is a response surface equation that relates the alternating strain to the number of cycles-to-crack initiation. The minimum life curve is three standard deviations below the average life curve and accounts for the data scatter caused by the effects of material property variability. Application of the minimum life curve yields a conservative estimate of the crack initiation life at a specified metal temperature.

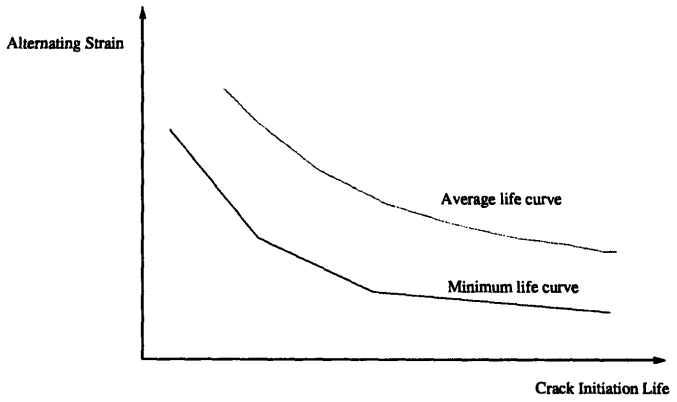

Figure 2-12: Crack Initiation Life Curves

The crack initiation life (N_f^{init}) , as predicted by the average life curve, is estimated using

$$log_{10}N_{f,i,j}^{init} = f_1(T_{mh,i,j}, T_3, \hat{\sigma}_{i,j}), \tag{2.36}$$

where T_{mh} is the hot-side liner temperature, T_3 is the compressor discharge temperature, and $\hat{\sigma}$ the equivalent stress. The equivalent stress, which is a function of the liner temperature, is estimated with the scaling formula proposed by Foltz and Kenworthy [25], as shown in

$$\frac{\hat{\sigma}_{i,j}}{\hat{\sigma}_{base,i,j}} = \frac{T_{mh,i,j} - T_3}{T_{base,i,j} - T_3}. \tag{2.37}$$

The baseline liner stress ($\hat{\sigma}_{base}$), and liner temperature (T_{base}) for each panel were calibrated using FLUENT and ANSYS data provided by an engine company [23].

2.5.2 Crack Propagation Life

The crack propagation life ($N^p_{f,i,j}$) was estimated using the following response surface equation,

$$log_{10} N^p_{f,i,j} = f_2(T_{mh,i,j}). \tag{2.38}$$

In Equation 2.38, the crack propagation life is a function of the metal temperature. This function was formed by performing a regression analysis on data for crack growth rates as a function of temperature for Hastelloy X [26].

2.5.3 Total Life

The total low-cycle fatigue life of the i^{th} panel and j^{th} cup section is determined from

$$N_{f,i,j} = (N^{init}_{f,i,j} + N^p_{f,i,j})(1 + \Psi), \tag{2.39}$$

where $N_{f,i,j}$ is the low-cycle fatigue life, and Ψ, the life curve multiplier (LCM), accounts for the effects of the material property variability. Ψ is set to zero during a deterministic analysis. For a probabilistic analysis, Ψ is represented by a normally-distributed random variable. Its standard deviation is determined from the data scatter about the average crack initiation life curve.

2.6 Summary

This chapter presented a simplified combustor model for estimating the metal temperature and the liner low-cycle fatigue life. The model contains four main elements: a network flow analysis, a lumped-parameter analysis of the combustor temperature field, a liner heat transfer analysis, and a low-cycle fatigue life analysis. The network flow analysis linked the mass flows across the crossing the liner to the bulk flow variability inside the liner. The lumped-parameter analysis of the temperature field provided estimates of the three driving temperatures: the effective radiation temperature, the near-wall gas temperature, and the cooling film temperature. A one-dimensional heat transfer model was used to estimate the liner temperature. Lastly, a low-cycle fatigue life model for the combustor liner was presented.

Chapter 3

Impact of Manufacturing Variability on Combustor Liner Durability

3.1 Introduction

This chapter presents a probability-based framework to quantify the impact of manufacturing variability on combustor liner durability. The impact of manufacturing variability on on the liner temperature and the liner life is estimated using a Monte Carlo analysis. Then, the Monte Carlo data are compared with the combustor rig and field failure data provided by an engine company. The lifing analysis was performed for two cases: I and II. In case I, the liner life distribution was driven by the liner temperature variability only. In case II, the effects of the material property variability were accounted for.

3.2 Manufacturing Variability

3.2.1 Random Variables

The combustor fabrication process produces variability in the part dimensions, material properties, and radial combustion gas temperature gradients. The effects of manufacturing variability are represented by independent, normally-distributed random variables, as shown in Figure 3-1. These random variables are the cooling slot metering hole diameter (δ_d), the slot height (s), the thermal barrier coating (TBC) surface emissivity (ε_{tbc}), the TBC thickness (t_{tbc}), the liner thickness (t_m), the bond coat thickness (t_{bnd}), the TBC thermal conductivity (k_{tbc}), the liner thermal conductivity (k_m), the bond coat thermal conductivity (k_{bnd}), the dome air flow rate (G_{air}), the fuel injector flow rate ($\dot{m}_{fuel}$), the combustor mixedness parameter (ζ), and the life curve multiplier (LCM) (Ψ). These parameters, with the exception of Ψ, are normalized by their mean values.

3.2.2 Nested Classes of Variability

The random variables are separated into two classes of variability: the cup-to-cup class (Class I) and the combustor-to-combustor class (Class II). Class I parameters exhibit vari-

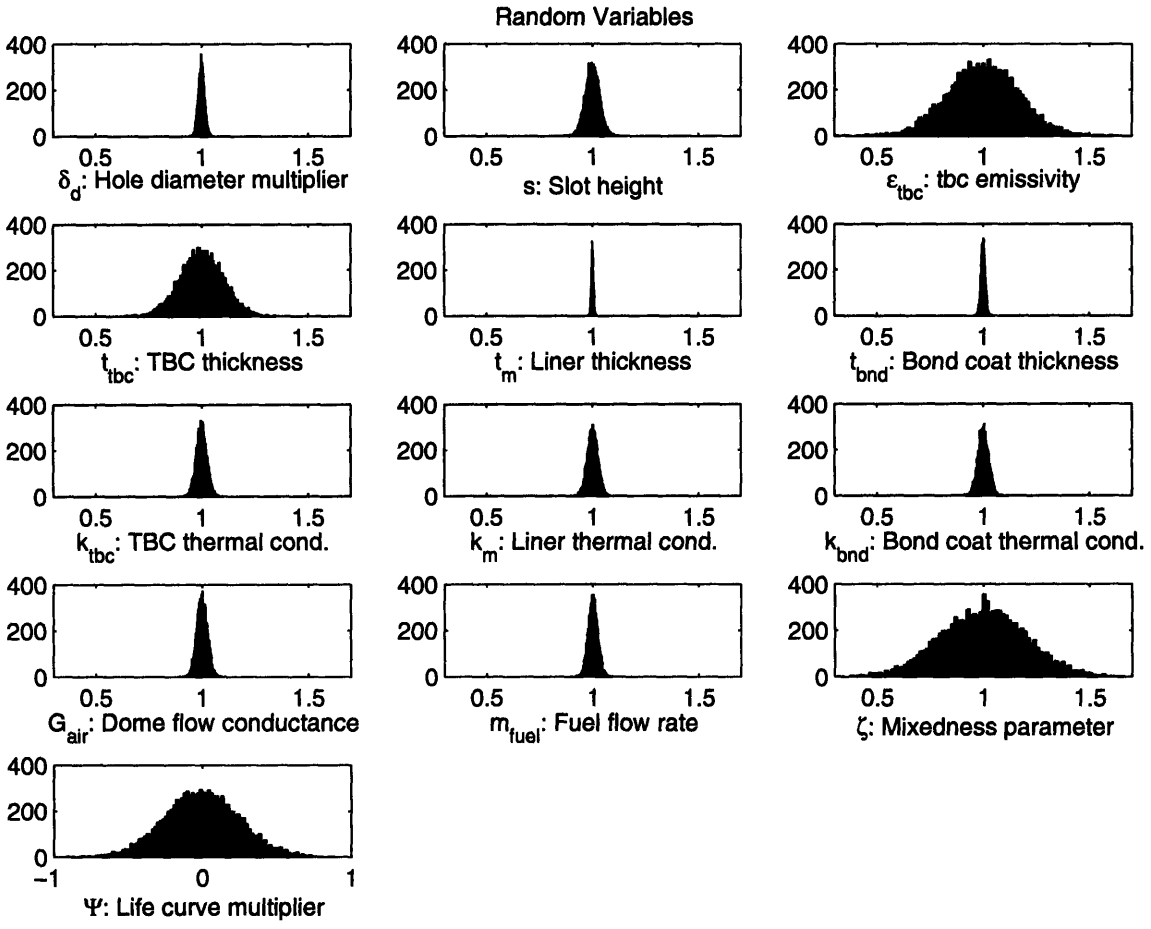

Figure 3-1: Random variables

ability from cup section to cup section within each combustor. Class II parameters predominately vary from combustor to combustor.

Class I: Cup-to-Cup Random Variables

Annular combustors consist of J air admission ports and fuel injectors at the front section of the combustor, or the dome. The flow characteristics of each port and fuel injector differ due to the variability of the part dimensions. As a result, the dome air flow and the fuel flow vary from cup to cup. The network flow model accounts for these effects.

The mean value of the dome air flow conductance was based on the nominal mass flow across the dome. The standard deviation of the dome air flow conductance determined from the flow tolerances of the air swirlers [34].

The mean and standard deviation of the fuel flow was determined from a nominal mass flow-pressure drop curve and its upper and lower 95-percent confidence bounds, as shown in Figure 3-2. These confidence bounds were based on fuel injector flow test limits specified by an engine company [34]. The mean fuel flow was set equal to the nominal fuel flow. The standard deviation is equal to one-half of the difference between the upper and lower 95-percent bounds on the fuel flow.

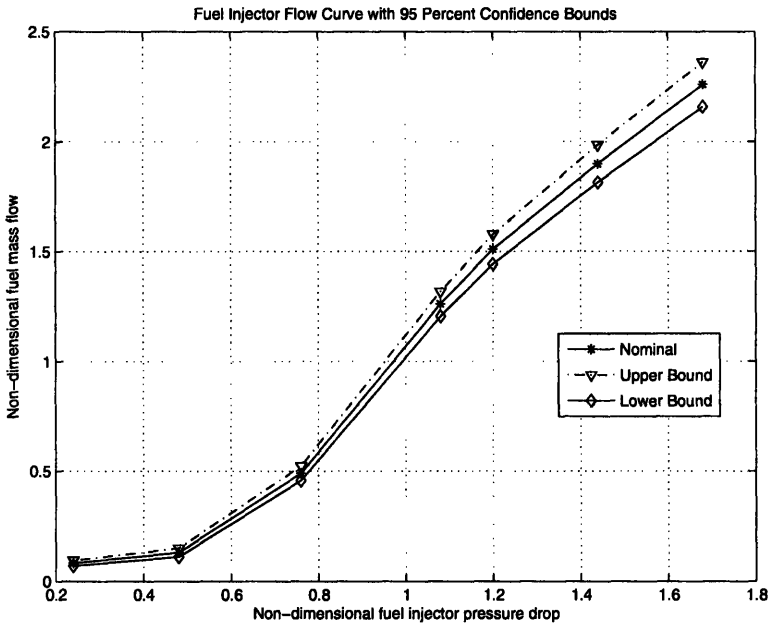

Figure 3-2: Fuel injector flow curve: mass flow vs. pressure drop

The combustor mixedness parameter accounts for the cup-to-cup variability of the radial gas temperature gradients within the combustor and the impact of these variations on the near-wall gas temperatures. The mean value and standard deviation of the mixedness parameter were determined from a statistical analysis of $\frac{T_{gas}-T_3}{T_{bulk}-T_3}$ combustor outlet temperature data obtained from a rig test [34, 23]. These outlet temperatures were measured with a rake consisting of five thermocouples that traversed the combustor exit plane in 3.6 degree increments, yielding 500 data points. The combustor annulus was divided into J regions corresponding with the J cup sections. The outlet near-wall gas temperatures for the inner

and outer liners were averageed within each cup section. The bulk gas temperature in each cup section was determined from a raw average, yielding a cup-to-cup distribution of g_2. The standard deviation of ζ was calibrated such that the probabilistic estimate of the g_2 standard deviation was equivalent to the statistical estimate obtained from the rig data.

Class II: Combustor-to-Combustor Random Variables

The combustor fabrication process produces cup-to-cup variability that is several orders of magnitude less than combustor-to-combustor variability [34]. Thus, these parameters were classified as Class II variables.

The film and dilution cooling holes were made using Electron Discharge Machine (EDM) drills. The EDM configuration minimized the variability of the hole dimensions on each combustor to several orders of magnitude less than the combustor-to-combustor variability. The variability of these holes is represented by δ_d, which varies all of the cooling holes from combustor to combustor during the probabilistic analysis. By updating the diameters of the film cooling holes and the dilution holes simultaneously, it is assumed that the variabilities of these hole sizes are perfectly correlated.

The nominal cooling slot height and its standard deviation were based on combustor design specifications. The slot was cut while the liner was being machined. Variability is introduced due to the process of setting up the combustor in the EDM. Thus, the predominant combustor-to-combustor variation of the slot height places it in Class II.

The material that comprised the TBC was approximately homogenous for each combustor. However, there are differences in this material from combustor to combustor. These differences yield combustor-to-combustor variations in the surface emissivity of the TBC. Similarly, the TBC thermal conductivity varies from combustor to combustor due to this effect. The nominal values of the TBC emissivity and its thermal conductivity were set to the design value. The standard deviations of these parameters were derived from their manufacturing tolerances.

The TBC and the bond coat were sprayed onto the combustor as it was turning circumferentially [34]. The spray process introduces combustor-to-combustor variability about the target TBC and bond coat thicknesses.

Combustor liners are typically comprised of Nickel-based alloys, such as Hastelloy-X and Nimonic 75 [1]. The liner thickness and its thermal conductivity exhibit variability from combustor to combustor. Similar to the cooling slot, the main source of the liner thickness variability can be attributed to the error in the orientation of the combustor during the machining process. The variation of the liner material among the combustors yields combustor-to-combustor variability of its thermal conductivity.

The effects of the material property variability on the low-cycle fatigue life is quantified by the life curve multiplier (Ψ). The material property variability is caused by the variability of the defect population in the liner material [30]. The manufacturing processes that produce combustor-to-combustor variability in the thermal conductivity of the metal also produce variability in its material properties. As a result, the LCM is classified as a Class II parameter [31]. The standard deviation of the crack initiation life is estimated by taking the difference between the average life and the minimum life then dividing the result by three. Dividing this quantity by the average life yields the coefficient of variation for the crack initiation life and is equal to the standard deviation of Ψ.

3.2.3 Hierarchical Analysis

A hierarchical analysis is used to account for these nested classes of variability for M combustors with J cup sections, as shown in Figure 3-3. First, each simulated combustor is assigned J fuel injectors and air admission ports at the front end. This configuration yields a distribution of fuel and air flow around the combustor annulus. Second, each combustor-to-combustor parameter has a value that is randomly sampled from its probability distribution. Third, these parameters are used to estimate the combustor liner temperatures and life using the combustor model. Finally, this process is repeated for the next $M - 1$ combustors to yield a liner life distribution for M combustors. These steps are integrated with a Monte Carlo analysis.

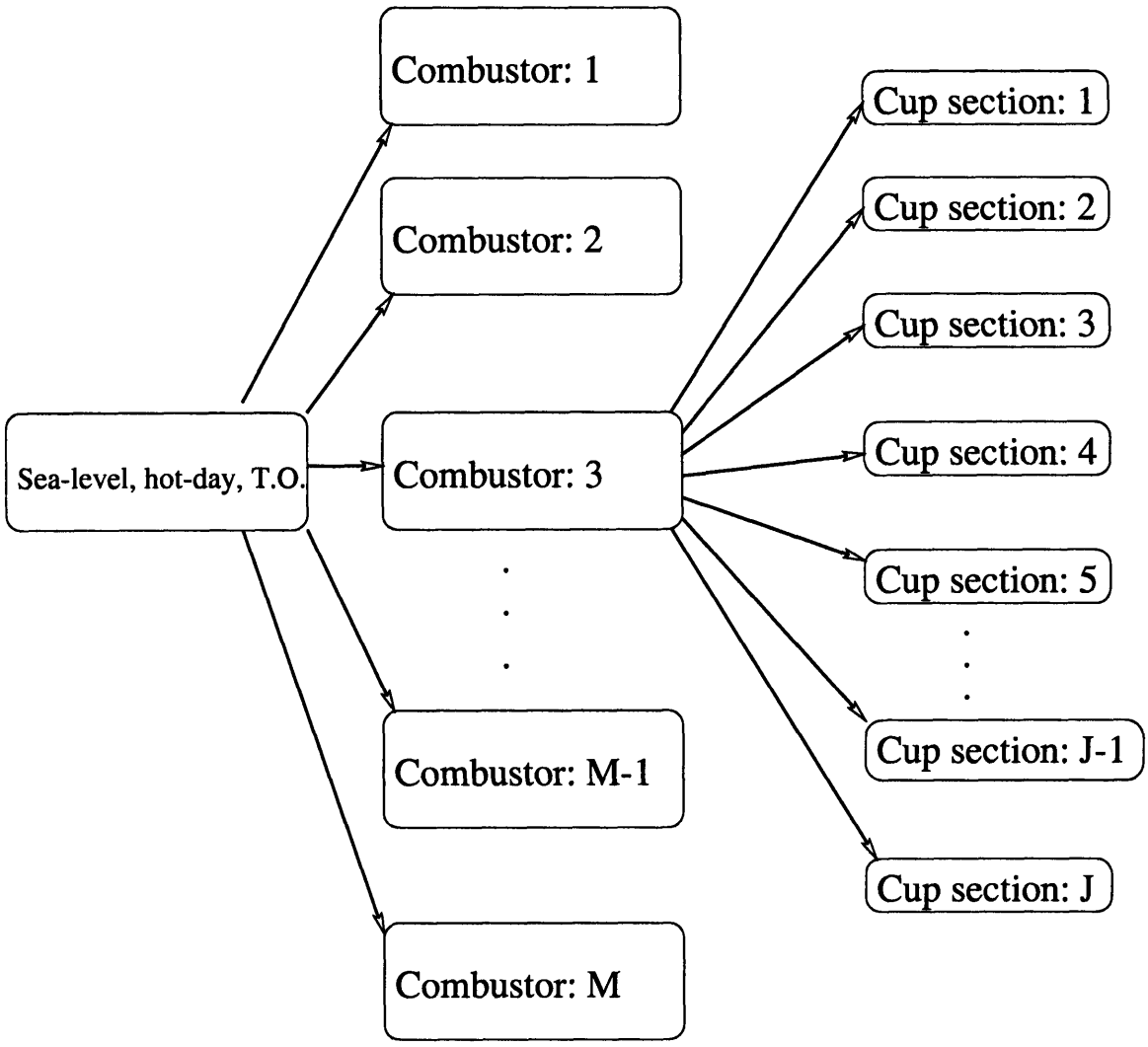

Figure 3-3: Hierarchical analysis for 'M' combustors and 'J' cup sections at sea-level, hot-day, take-off operating condition.

3.3 Model Assessment

A Monte Carlo analysis was applied to the simplified models of combustors A and B, and the results were compared with a statistical analysis of the bulk gas temperature distribution at the combustor outlet, the liner wall temperature measurements, and the field failure data provided by an engine company [32].

3.3.1 Combustor Outlet Bulk Gas Temperatures

A comparative analysis of the bulk temperature variability at the combustor outlet was performed to assess the network flow model. Specifically, probabilistic estimates of the coefficient of variation of the combustor temperature rise ($T_4 - T_3$) for combustors A and B was compared with statistical estimates of the bulk temperature variability obtained from combustor rig tests. For each combustor, the probabilistic estimate was calculated from a 1,000-trial Monte Carlo simulation, where the coefficient of variation of the combustor temperature rise was determined for each trial.

The assessment was made with the rig data referred to in Section 3.2.2. The description of the data is restated here. A rake with five thermocouples traversed the combustor exit plane in 3.6 degree increments, yielding 500 data points. The combustor annulus was divided into J regions corresponding with the J cup sections. The data points in each cup section were averaged to compute the outlet bulk gas temperature for each cup section, and this analysis yielded J outlet bulk temperatures. Then, the coefficient of variation of the J bulk temperatures at the outlet were determined.

The outlet bulk temperature variabilities determined from the rig data are within the 2.5- and 97.5-percentile values of the probabilistic estimates for combustors A and B, as shown in Figures 3-4 and 3-5. These results show that the probabilistic estimates of the bulk temperature variability of the outlet are consistent with the statistical estimates from the combustor rig data, which validates the application of the network flow model for determining the cup-to-cup bulk gas temperature variability.

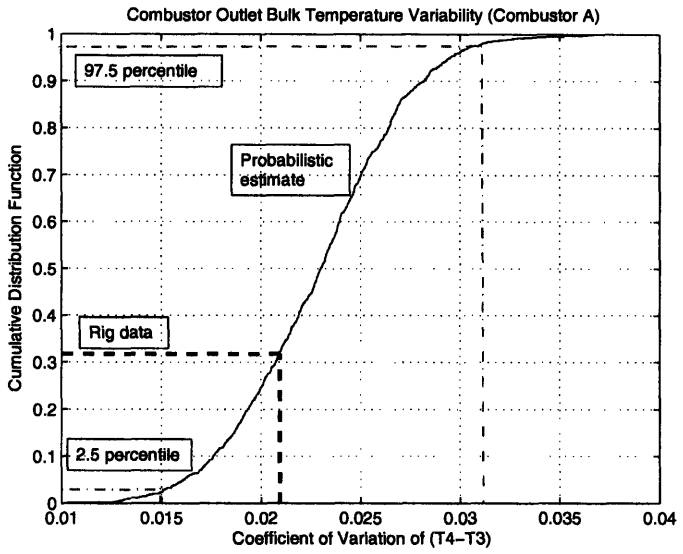

Figure 3-4: Combustor A outlet bulk temperature variability

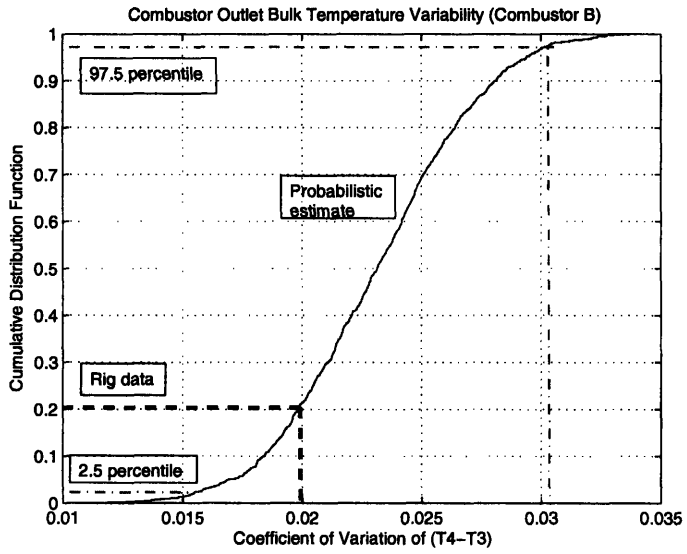

Figure 3-5: Combustor B outlet bulk temperature variability

3.3.2 Combustor Liner Temperatures

The probabilistic estimates of the combustor liner temperatures determined from 1,000-trial Monte Carlo simulations were compared with wall temperature measurements acquired from separate rig tests for combustors A and B. However, the lack of available data the makes the comparison of the probabilistic estimates to the liner temperature data more problematic than the outlet bulk temperature comparison.

Combustor A

Liner wall temperature measurements for combustor A were acquired from a rig test. The thermocouples were placed on hot spots, or elevated-temperature areas, that were previously identified using thermal paint [19]. In particular, the hot spots were located in four to eight separate cup sections for panels one through four. The inner and outer liner wall temperature measurements for each panel were lumped together prior to the statistical analysis due to the small amount of available data. These measurements were averaged within cup section in order to yield a single temperature. The mean and standard deviation of the temperature difference between the thermocouple measurements and a reference temperature (T^o_{mh}) for each combustor A panel were computed and then compared to the probabilistic model estimates, as shown in Figure 3-6. The probabilistic estimates of the mean and standard deviation of the liner temperatures for panels one, two, and four fall outside of the 95 percent confidence bounds of the thermocouple data. The mean liner temperature estimate falls within these confidence bounds for the panel three data. The estimate of the liner temperature standard deviation is approximately 1 to 2 degrees K less than the lower confidence bound on the standard deviation of the thermocouple data for panels one and two. For panel three, the model estimate of the standard deviation is approximately 12 degrees K less than the lower confidence bound on the estimate from the thermocouple data. The model estimate of the standard deviation falls within the confidence bounds of the thermocouple data. Overall, the probabilistic model underestimates the cup-to-cup liner temperature variability compared to the variability estimated from the thermocouple data.

Combustor B

There was little available data on the liner temperatures for combustor B. Specifically, the thermocouple measurements of the inner and outer liner temperatures were acquired from a single cup section [23]. Two thermocouples were placed in panels one, three, and four, and one thermocouple was placed in panel two. As a result, a direct comparison of the model estimate of the cup-to-cup liner temperature variability and the statistical estimate from the thermocouple data could therefore not made. The probabilistic estimates of the mean combustor B liner temperatures and the corresponding 95-percent confidence bounds were compared with the thermocouple data, as shown in Figure 3-7. For the outer liner, the probabilistic estimate of the mean liner temperatures deviate from the thermocouple data by approximately 50 to 160 degrees K for panels one through four. For the inner liner, the probabilistic estimate is within 10 degrees K of the thermocouple data for panels two and three. In addition, the probabilistic estimate exceeds the estimate from the thermocouple data by approximately 60 to 120 degrees K for panels one and four.

3.3.3 Discussion

The rig data do not represent perfect estimates of the liner temperature variability. These liner data were not collected for the purpose of assessing this model, but rather were data that happened to be available from prior testing of the combustor. They do not present an ideal data set. For a statistical analysis, the thermocouples in each cup section should have been assigned to coordinates that were fixed relative to each fuel injector to mitigate the influence of circumferential and longitudinal metal temperature gradients on the wall temperature measurements. The paucity of data resulted in the inner and outer liner temperatures measurements being lumped into the same data set prior to the statistical analysis of combustor A. In addition, the thermocouples were placed in a single cup section over four panels for combustor B. As a result, a comparison of the probabilistic estimate of the cup-to-cup wall temperature variability to a statistical analysis of the data was not performed.

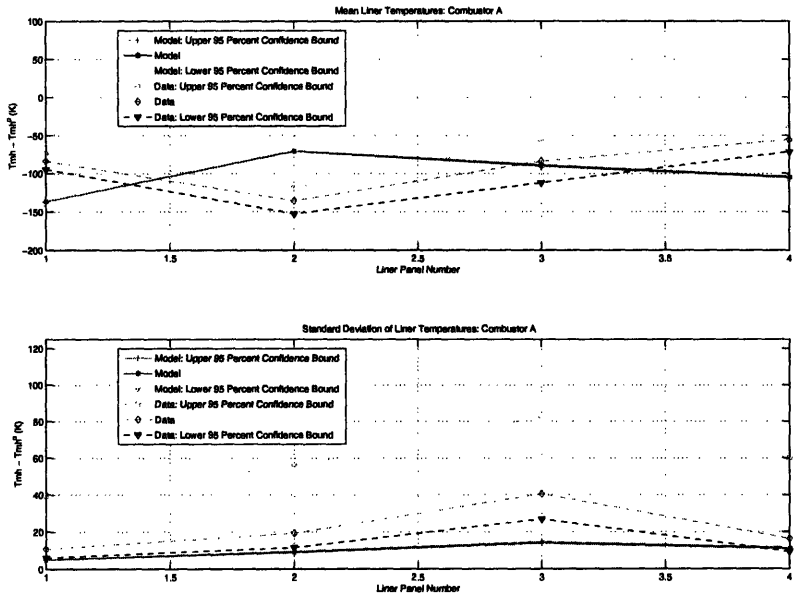

Figure 3-6: Combustor A liner temperatures

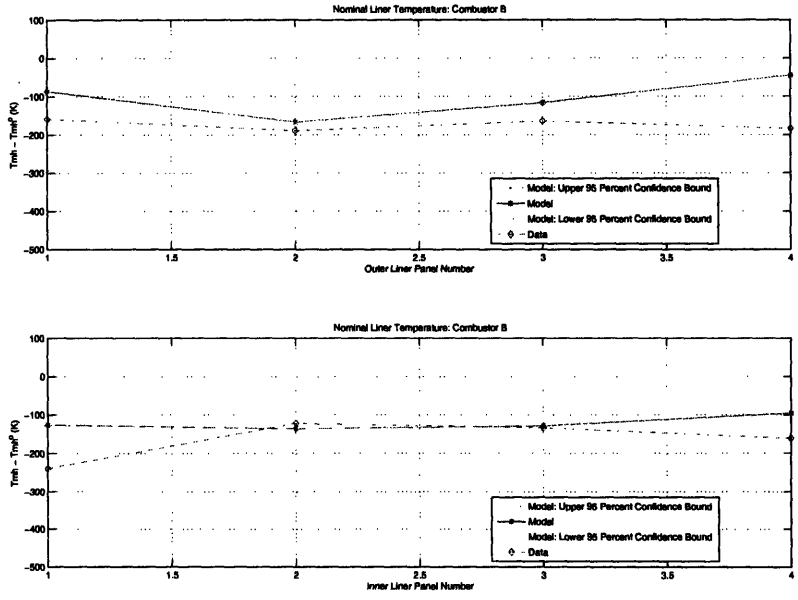

Figure 3-7: Combustor B liner temperatures

3.3.4 Combustor Liner Life

The probabilistic estimates of the liner life distributions for combustors A and B are presented in this section. 10,000-trial Monte Carlo analyses were performed for two cases: I and II. In case I, the liner life variability was caused by the liner temperature variations estimated by the model. In case II, the effects of the material property variability were accounted for. These analyses were performed separately to quantify the impact of the liner variability and the material property variability on the combustor liner life distribution. The minimum (B_1) combustor life and the typical (B_{50}) combustor life were estimated in both cases. The B_1 life and the B_{50} life are defined as the number of cycles until one percent and 50 percent of the combustors fail, respectively.

Case I: Impact of Aerothermal Variability on Combustor Liner Life

The impact of aerothermal variations due to known sources of manufacturing variability is to increase the likelihood that combustors designed to the nominally calculated life will fail earlier than predicted using deterministic methods. The difference between life distribution and the nominal life divided by the nominal life is shown in Figure 3-8, and the life distribution divided by the nominal life is shown in a Weibull scale in Figure 3-9. In Figure 3-8, a value of zero indicates that the typical liner life is equal to the nominal life. This figure shows that the typical liner life is approximately 22 percent less than the nominal life. Furthermore, the probability that a randomly selected combustor will have a life that is less than the nominal life is approximately 99 percent. The life distribution is not linear on the Weibull scale, as shown in Figure 3-9. The curvature in the plot indicates that the CDF is not consistent with a Weibull distribution.

The impact of aerothermal variability on the combustor B liner life is shown in Figures 3-10 and 3-11. The results are similar to combustor A showing that the typical life is 17 percent less than the nominal life, and that 99 percent of all liners will have a life less than the nominal. Furthermore, the combustor B life distribution is not consistent with a Weibull distribution.

The mean shift occurs because the combustor liner life is the lowest life for all sections of the liner. Liner temperature variability within each combustors yields a liner temperature distribution with finite variance. As a result of these conditions, the life distribution for a fleet of combustors is driven by the lower tail of the liner life distribution with each combustor. Increased aerothermal variability decreases the values in the lower tail of the life distribution within each combustor. Therefore, the median value of the combustor life distribution for the fleet must also decrease.

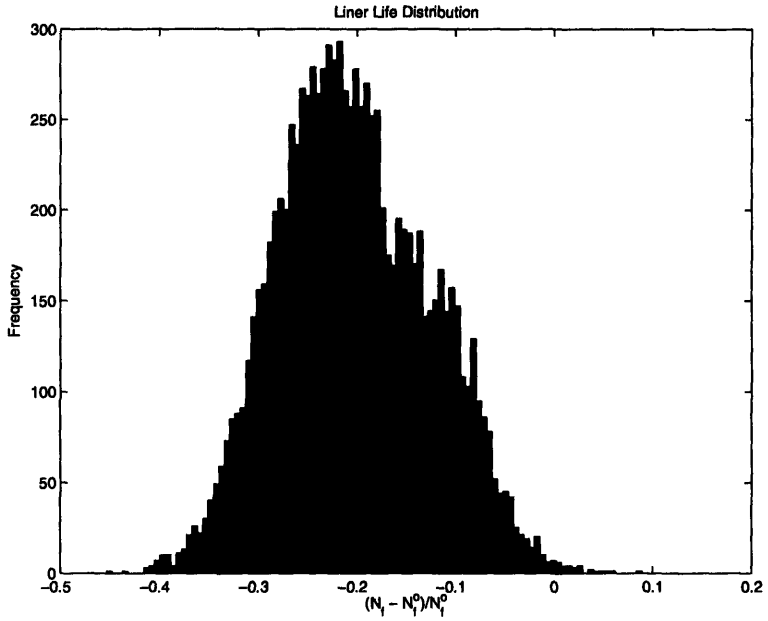

Figure 3-8: Case I (without material property variability): combustor A life PDF

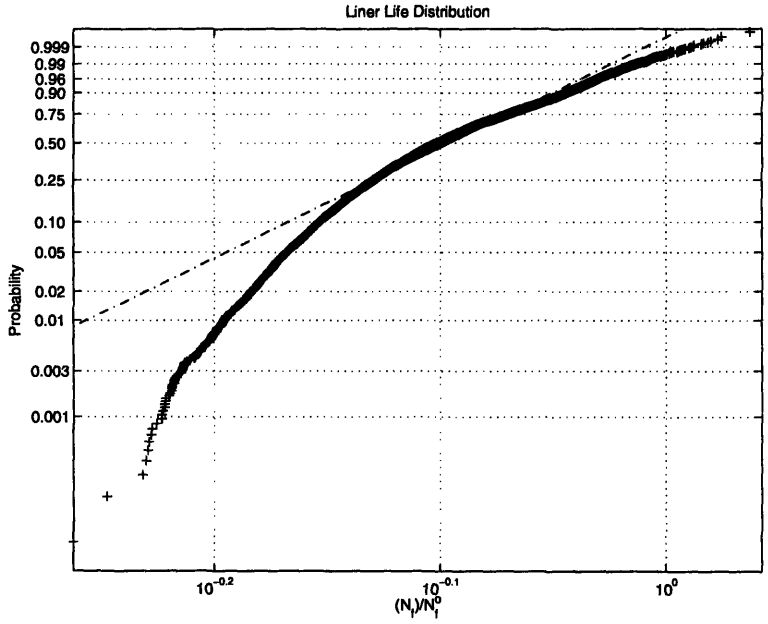

Figure 3-9: Case I (without material property variability): combustor A life CDF on a Weibull scale

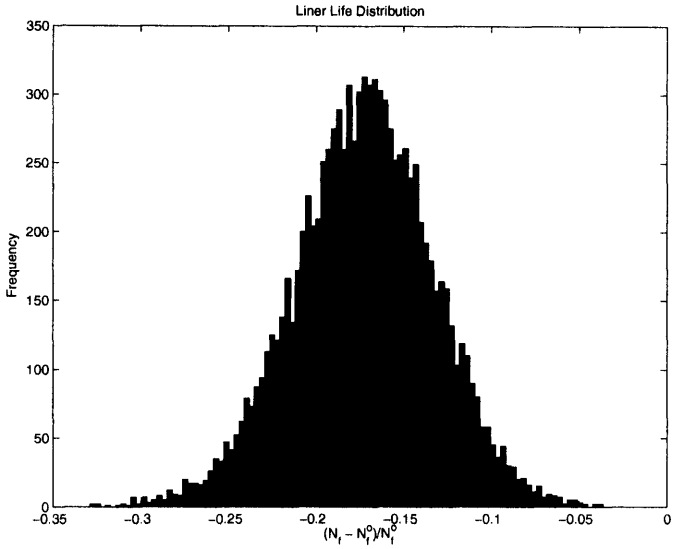

Figure 3-10: Case I (without material property variability): combustor B life PDF

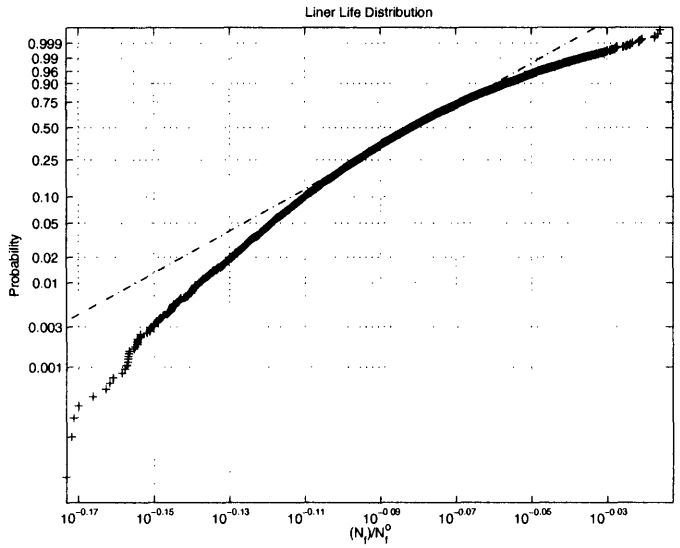

Figure 3-11: Case I (without material property variability): combustor B life CDF on a Weibull scale

Case II: Impact of Material Property Variability on Combustor Liner Life

Figures 3-12 and 3-13 show the probability density function and the cumulative distribution function for the life distribution when the material property variations are accounted for in the probabilistic analysis. The cumulative distribution functions for combustors A and B are consistent with a Weibull distribution. For combustor A, the typical life is 20 percent less than the nominal life, and the probability that a particular combustor will fail earlier than predicted using a deterministic calculation is 80 percent. For combustor B, typical life is approximately 20 percent less than the nominal life, and the probability that any given combustor will fail earlier than predicted using a deterministic analysis is approximately 80 percent. Incorporating the material property variability into the probabilistic analysis does not impact of the typical life.

The variability of the life distribution is greater in Case II than in Case I. Specifically, the combustor A minimum life decreases by 48 percent of the Case I value, and the combustor B minimum life decreases by 51 percent of the Case I value when the material property variability is included. The impact of the material property variability on the combustor liner durability is noteworthy because the maintenance schedules of the part is based on the minimum life. As such, reducing the magnitude of the material property variability would increase the minimum combustor life.

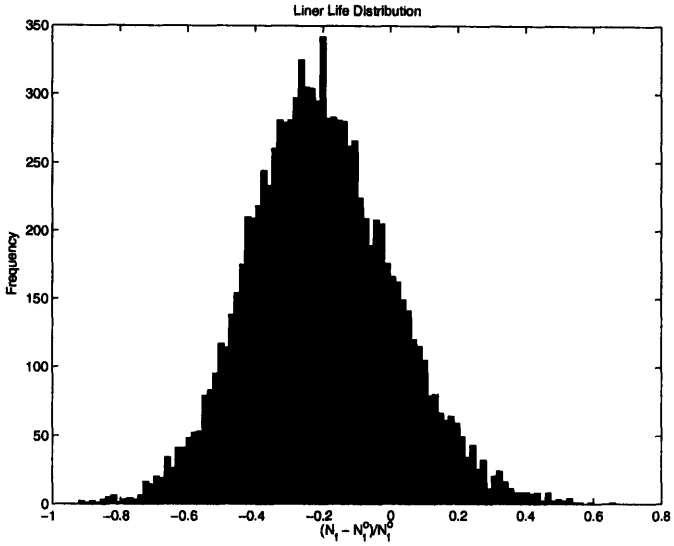

Figure 3-12: Case II (with material property variability): combustor A PDF

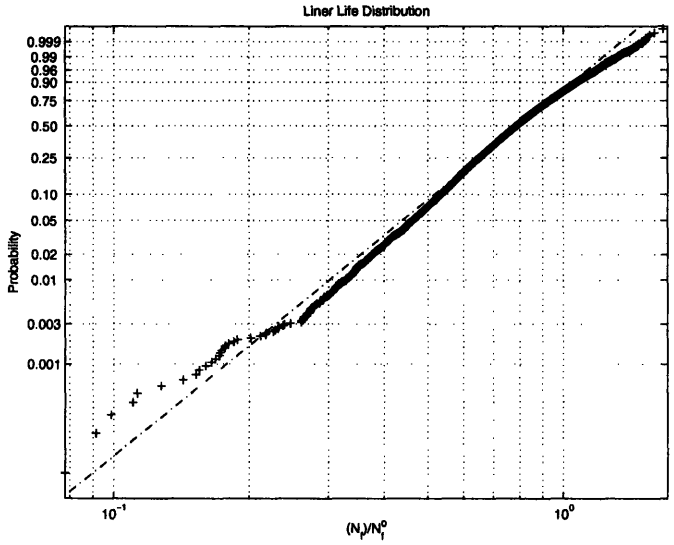

Figure 3-13: Case II (with material property variability): combustor A CDF on a Weibull scale

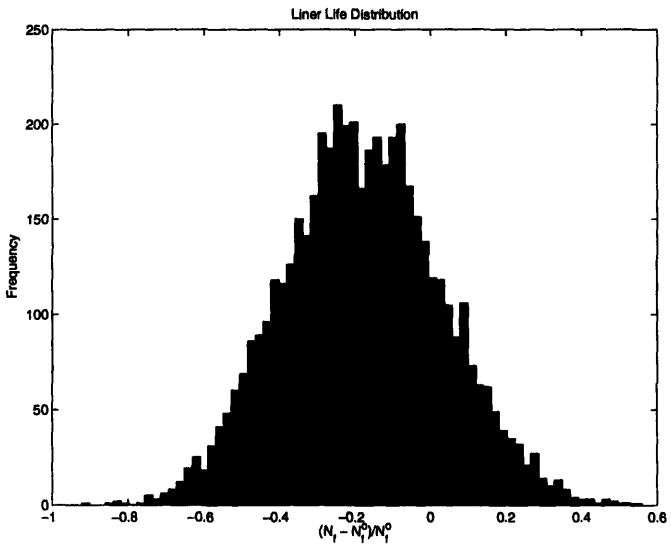

Figure 3-14: Case II (with material property variability): combustor B life PDF

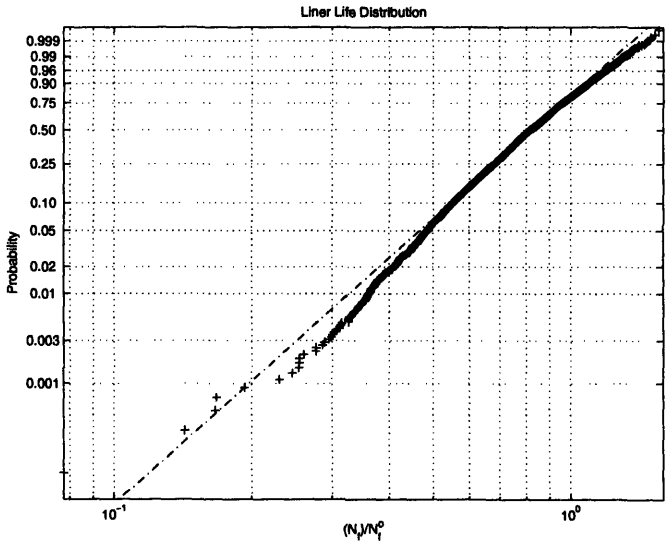

Figure 3-15: Case II (with material property variability): combustor B life CDF on a Weibull scale

Comparison to Field Data

Table 3.1 presents a comparison of the parameters determined from a Weibull analysis of the combustor B field data and from the probabilistic analysis. These parameters are the coefficient of variation of the life distribution (V_{N_f}) and the Weibull distribution shape parameter (β). The probabilistic model estimate of the coefficient of variation is 20 percent and 100 percent of the field data values for cases I and II, respectively. Furthermore, the shape parameter, another measure of the variability of a Weibull distribution, is 96 percent of the field data value. Thus, incorporating the effects of the material property variability into the lifing analysis yields an accurate estimate of the variability in the combustor B field failure data.

Table 3.1: Comparative Analysis of Combustor B Life

Parameter	Case I	Case II
V_{N_f}	0.20	1.00
β	–	0.96

3.4 Conclusions

This chapter presented a probability-based framework for quantifying the impact of manufacturing variability on combustor outlet temperature, liner temperature, and liner life. The probabilistic analysis showed that the typical combustor life and the variability of the combustor liner life were functions of the liner temperature variability and the material property variability, respectively. The liner temperature estimates from the model were applied to a low-cycle fatigue life analysis, which yielded combustor life distributions for both combustors. Two cases were run. The first case did not account for the effects of the material property variability, and the probabilistic estimate of the typical lives were approximately 19 and 17 percent less than the nominal life estimate for combustors A and B, respectively. In second case, the effects of the material property variability were included, and the probabilistic estimate of the typical lives were approximately 22 and 17 percent less than the nominal lives for combustors A and B, respectively. Furthermore, the probabilistic estimate of the combustor B life yielded a coefficient of variation that was approximately 20 percent and 100 percent of the field data values for cases I and II. Thus, the probabilistic model underestimates the variability present in the field failure data when the material property variability is not included and accurately approximates the variability these effects are incorporated. Finally, a comparative analysis showed that the material property variations accounted for 80 percent of the combustor B life variability while the liner temperature variability only accounts for 20 percent of the combustor B life variability.

Chapter 4

Sensitivity Analysis

4.1 Introduction

This chapter presents a methodology for determining the leading drivers of the combustor liner life. A regression analysis is applied to the Monte Carlo data in order to establish a simplified representation of the relationship between the combustor liner life in each cup section and the random variables introduced in Chapter 3. This surrogate model is subsequently used to identify the leading drivers of the liner life. Specifically, the impact of increasing and decreasing the manufacturing tolerances on the combustor liner life distribution is quantified. Applying a surrogate model for the life enables an execution of several sensitivity studies at a lower computational expense than directly applying the combustor model.

4.2 Response Surface Analysis

A quadratic response surface equation is

$$Y = a_0 + \sum_{n=1}^{N} b_n \hat{x}_n + \sum_{n=1}^{N} c_n \hat{x}_n^2, \tag{4.1}$$

where Y is the response, $\hat{x}_n$ is n^{th} random input, and N is the number of random inputs. The regression coefficients, a_0, b_n, and c_n, are solved in a least squares sense. The response surface is fitted to M data points and is written in matrix form in order to solve for the regression coefficients in

$$\underline{Y} = \underline{X}\beta + \underline{\varepsilon}, \tag{4.2}$$

where $\underline{Y}$ is response, $\underline{X}$ is the matrix of the levels of the regressor variables, β is the vector of regression coefficients, and $\underline{\epsilon}$ is the vector of random errors [35]. The elements of these parameters are shown in the following equations

$$\underline{Y} = \begin{bmatrix} y_1 \\ y_2 \\ . \\ . \\ . \\ y_M \end{bmatrix} \tag{4.3}$$

$$\underline{X} = \begin{bmatrix} 1 & \hat{x}_{1,1} & \dots & \hat{x}_{N,1} & \hat{x}_{1,1}^2 & \dots & \hat{x}_{N,1}^2 \\ 1 & \hat{x}_{1,2} & \dots & \hat{x}_{N,2} & \hat{x}_{1,2}^2 & \dots & \hat{x}_{N,2}^2 \\ . & . & . & . & . & & \\ . & . & . & . & . & & \\ . & . & . & . & . & & \\ 1 & \hat{x}_{1,M} & \dots & \hat{x}_{N,M} & \hat{x}_{1,M}^2 & \dots & \hat{x}_{N,M}^2 \end{bmatrix} \tag{4.4}$$

$$\beta = \begin{bmatrix} a_0 \\ b_1 \\ . \\ . \\ b_N \\ c_1 \\ . \\ . \\ c_N \end{bmatrix} \tag{4.5}$$

$$\underline{\epsilon} = \begin{bmatrix} \epsilon_1 \\ \epsilon_2 \\ . \\ . \\ . \\ \epsilon_N \end{bmatrix}. \tag{4.6}$$

The least squares estimators of Equation 4.2 are determined by minimizing the following equations [35]:

$$L = \sum_{j=1}^{n} \epsilon_j^2 = \underline{\epsilon}^T \underline{\epsilon} \tag{4.7}$$

and

$$L = \underline{Y}^T \underline{Y} - 2\beta^T \underline{X}^T \underline{Y} + \beta^T \underline{X}^T \underline{X} \beta. \tag{4.8}$$

Taking the partial derivative of L with respect to β and setting the result equal to zero yields

$$\frac{\partial L}{\partial \beta} = -2\underline{X}^T \underline{Y} + 2\underline{X}^T \underline{X} \beta = 0. \tag{4.9}$$

Rearranging terms yields a compact form of the normal equations

$$\underline{X}^T \underline{X} \hat{\beta} = \underline{X}^T \underline{Y}, \tag{4.10}$$

where $\hat{\beta}$ is the least squares solution.

4.2.1 Application to Monte Carlo Data

The response surface analysis is applied to the Monte Carlo data. The first step is to separate the liner life data by cup section. Second, a regression analysis is applied to the life distribution of the j^{th} cup section, input parameters 1 to 12 for the j^{th} cup section. The data are fitted to a quadratic, multi-variate response surface equation

$$Y_j = a_{0,j} + \sum_{n=1}^{12} b_{n,j}\hat{x}_{n,j} + \sum_{n=1}^{12} c_{n,j}\hat{x}_{n,j}^2, \tag{4.11}$$

where Y_j, the standardized random variate for the natural logarithm of liner life for the j^{th} cup section, is determined from

$$Y_j = ln(N_{f_j}), \tag{4.12}$$

and $\hat{x}_{n,j}$, the n^{th} standardized random input in the j^{th} cup section, is determined from

$$\hat{x}_{n,j} = \frac{x_{n,j} - \mu_n}{\sigma_n}. \tag{4.13}$$

Third, the adequacy of the response surface fit is checked. These response surface equations capture most of the variability exhibited in the Monte Carlo data. The coefficient of multiple determination quantifies the proportion of variability explained by the response surface equation. It is approximately 97 percent and 93 percent for the combustor A and B response surfaces, respectively. Furthermore, the percent errors of the standard deviation estimated by the response surfaces are 2 and 4 percent for combustors A and B, respectively.

Each regression coefficient exhibits cup-to-cup variability. This source of this variability is sampling error. The variability of the coefficients implies that the cup sections will yield different nominal values of liner life for the same inputs. Ideally, the nominal cup section lives would be identical for the same inputs.

There are two ways to mitigate the effects of sampling error. The first approach consists of increasing of the number of trials run in the Monte Carlo analysis. However, the slow convergence of the Monte Carlo simulation increases the computational expense of this option. An alternative approach is to define the response surface based on cup-average regressors. In other words, each regression coefficient was averaged over J cups. The averaged coefficients are determined from

$$\bar{a}_0 = \frac{1}{J}\sum_{j=1}^{J} a_{0,j} \tag{4.14}$$

$$\bar{b}_n = \frac{1}{J}\sum_{j=1}^{J} b_{n,j} \tag{4.15}$$

$$\bar{c}_n = \frac{1}{J}\sum_{j=1}^{J} c_{n,j}. \tag{4.16}$$

The averaging procedure yields

$$ln(N_{f,j}) = \bar{a}_0 + \sum_{n=1}^{12} \bar{b}_n \hat{x}_{n,j} + \sum_{n=1}^{12} \bar{c}_n \hat{x}_{n,j}^2, \tag{4.17}$$

a response surface for the life that uniformly responds to perturbations of the inputs. The liner life of the j^{th} cup section is estimated using

$$N_{f,j} = \exp\left(\bar{a}_0 + \sum_{n=1}^{12} \bar{b}_n \hat{x}_{n,j} + \sum_{n=1}^{12} \bar{c}_n \hat{x}_{n,j}^2\right)(1 + \Psi), \tag{4.18}$$

where Ψ incorporates the effects of the material property variability. Equation 4.18, which determines the life distribution of the j^{th} cup section for M combustors, is then post-processed to yield the total combustor life distribution.

4.3 Impact of Tightening Manufacturing Tolerances

A one-at-time (OAT) sensitivity analysis was applied to the response surfaces to quantify the impact of changing the input variations on the life distribution. The standard deviation of each random variable was reduced by a pre-determined amount while holding the remaining parameter standard deviations constant. Next, a Monte Carlo analysis consisting of 50,000 trials was performed with the updated standard deviations of these parameters. Then, the combustor life was computed by taking the minimum value of the response surfaces over J cups for each combustor. The B_1 and B_{50} lives of M combustors were estimated for each case. These estimates were compared with the Monte Carlo results presented in Chapter 3. The B_1 and the B_{50} lives were normalized by the nominal life and presented on bar graphs. Two cases were run for each combustor, as shown in Table 4.1. The input standard deviations were decreased by 90 and 50 percent for cases one and two, respectively.

Table 4.1: Sensitivity Analysis: Tightening Tolerances

Case	Percent Decrease
1	90
2	50

4.3.1 Case 1: 90-percent tolerance reduction

Combustor A

Decreasing the input standard deviations in a one-at-a-time fashion by 90 percent increases the B_1 and the B_{50} lives, as shown in Figures 4-1 and 4-2. Specifically, the combustor A B_1 life increases by approximately 33 percent of the nominal life when the standard deviation of Ψ is reduced by 90 percent. The B_1 life increases by less than 3 percent of the nominal life when the standard deviations of parameters 1 through 12 are reduced by 90 percent. Futhermore, the combustor A B_{50} life increases by approximately 6 percent of the nominal life when the standard deviation of ζ is reduced by 90 percent. Reducing the variability of Ψ by 90 percent changes the B_{50} life by less than one percent of the nominal life. The

results show that Ψ and ζ are the leading drivers of the B_1 life and B_{50} life, respectively, for combustor A.

Combustor B

Figures 4-3 and 4-4 show decreasing the variability of Ψ by 90 percent yields a B_1 life increase of approximately 25 percent of the nominal life and a B_{50} life increase of approximately one percent of the nominal life for combustor B. Also, decreasing the variability of ζ by 90 percent increases the combustor B B_1 life and B_{50} life by approximately 7 percent and 17 percent of the nominal life, respectively. The results show that Ψ and ζ are the leading drivers of the B_1 life and B_{50} life, respectively, for combustor B.

4.3.2 Case 2: 10-percent tolerance reduction

Combustors A

The standard deviations of the inputs were reduced by 10 percent of the original values in Case 2. Figure 4-5 shows that the combustor A B_1 life increases by approximately 5 percent of the nominal life when the standard deviation of Ψ is reduced by 10 percent and that reducing the standard deviations of parameters 1 to 11 yielded B_1 life increases of less than one percent. Figure 4-6 shows that the B_{50} increases by less than one percent of the nominal life when the standard deviations of all of the random variables are increased in an OAT fashion.

Combustor B

The combustor B B_1 and B_{50} life increases were negligible compared to the nominal life when the variabilities of parameters 1 to 11 were decreased by 10 percent, as shown in Figures 4-7 and 4-8. The B_{50} life increases by approximately 3 percent when the standard deviation of Ψ is decreased by 10 percent, and the B_1 life increases by approximately 3 percent when the standard deviation of ζ is decreased by 10 percent.

Discussion: Cases 1 and 2

The sensitivity analysis shows that the leading drivers of the minimum combustor life and the typical combustor life are the material property variability and the combustor mixedness variability, respectively. A robust design that improves combustor liner durability would consist of a liner material with less material property variability than currently used on combustors A and B. Furthermore, a combustor configuration that increases the consistency of the combustor mixedness levels from cup to cup would decreases the liner temperature variability, and, in turn, would increases the typical combustor life.

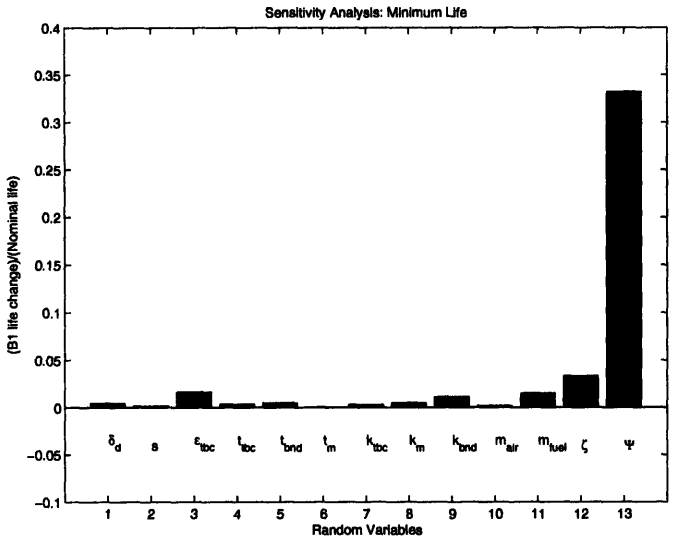

Figure 4-1: Combustor A: B_1 life change for 90 percent tolerance decrease.

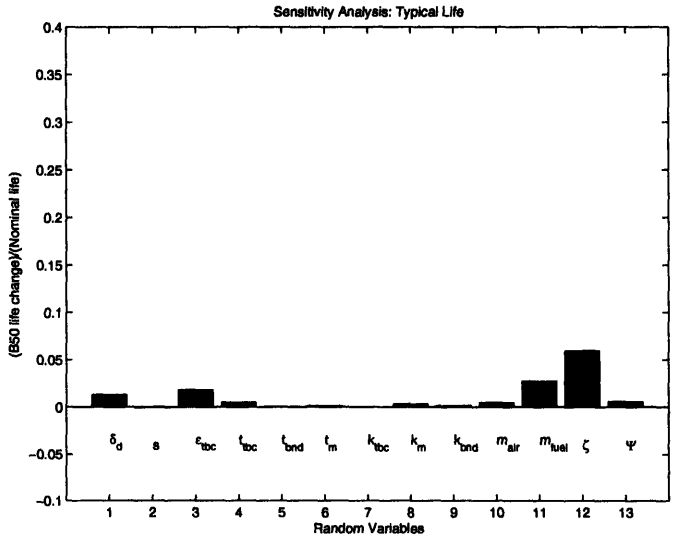

Figure 4-2: Combustor A: B_{50} life change for 90 percent tolerance decrease.

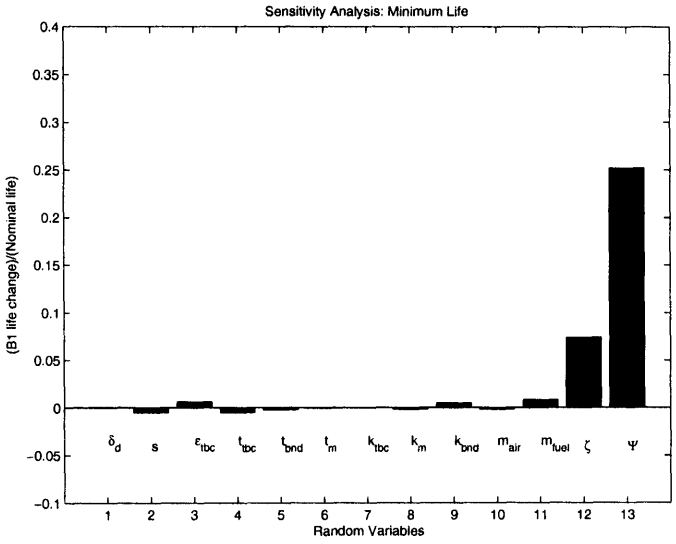

Figure 4-3: Combustor B: B_1 life change for 90 percent tolerance decrease.

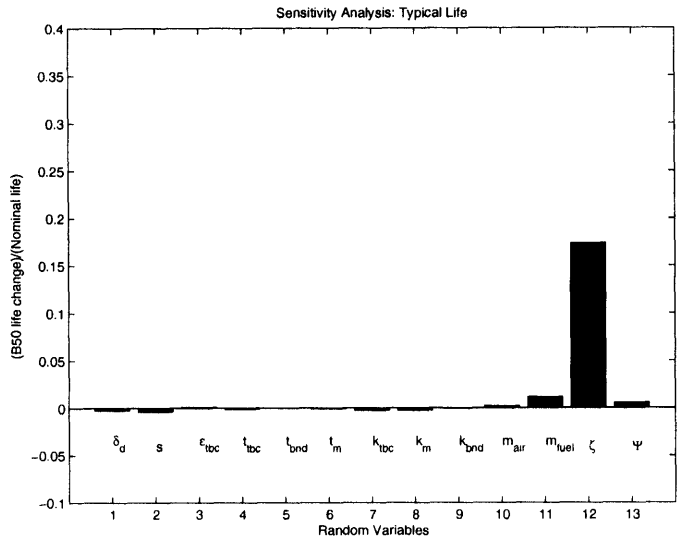

Figure 4-4: Combustor B: B_{50} life change for 90 percent tolerance decrease.

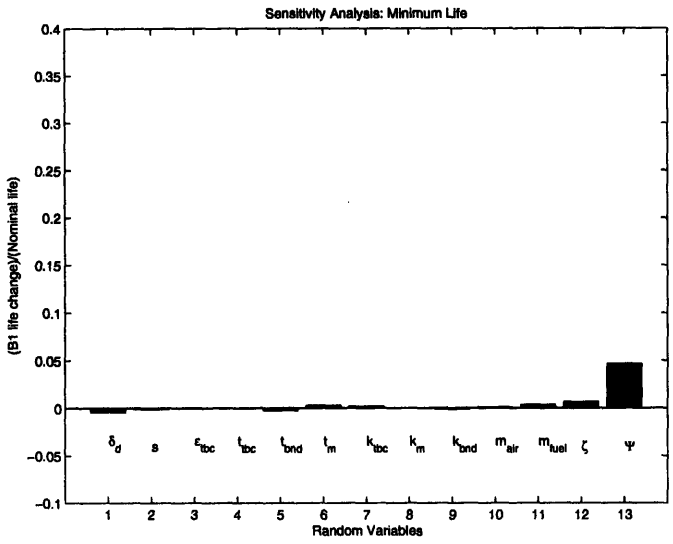

Figure 4-5: Combustor A: B_1 life change for 10 percent tolerance decrease.

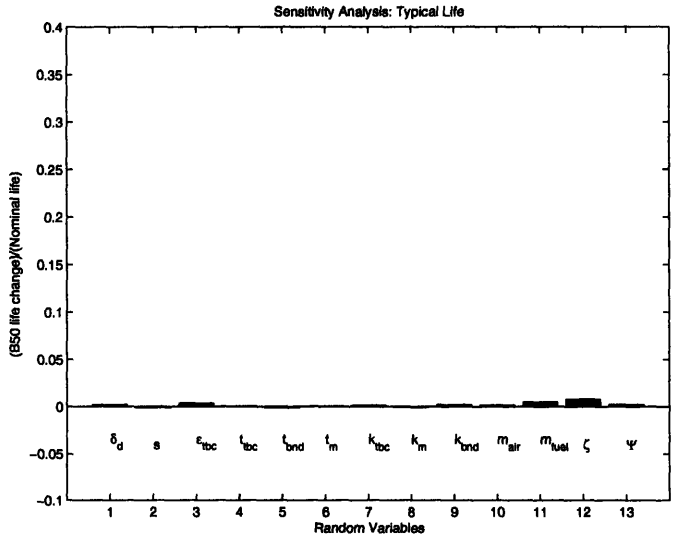

Figure 4-6: Combustor A: B_{50} life change for 10 percent tolerance decrease.

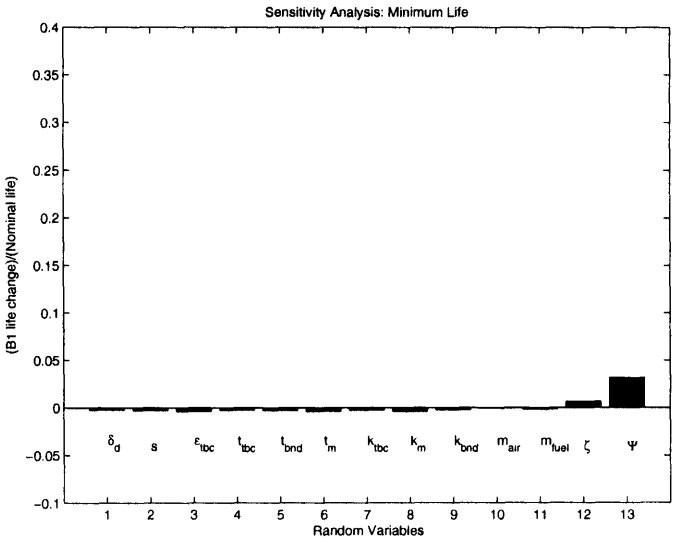

Figure 4-7: Combustor B: B_1 life change for 10 percent tolerance decrease.

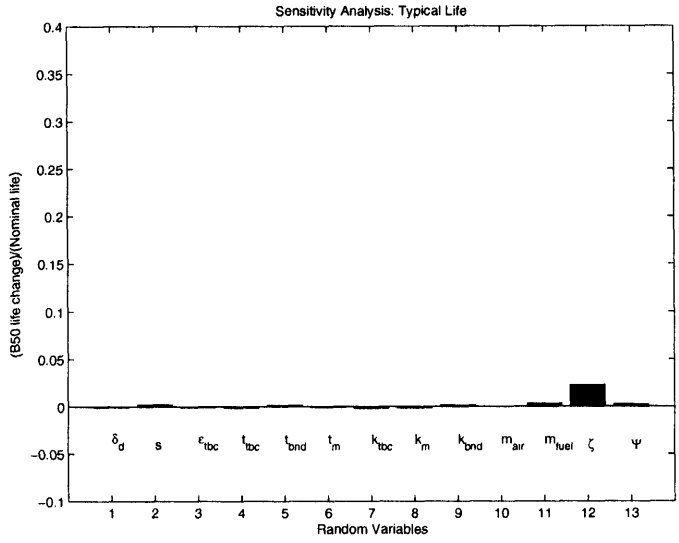

Figure 4-8: Combustor B: B_{50} life change for 10 percent tolerance decrease.

4.4 Impact of Opening Manufacturing Tolerances

An OAT sensitivity analysis was also conducted in order to quantify the impact of increasing the input parameter variations on the life distribution. Increasing the input parameter variability simulates the effects of loosening the manufacturing tolerances of each parameter. These actions will decrease the minimum and typical lives of the fleet. One case were run for each combustor, where the input standard deviations were increased by 10 percent of their original values.

Increasing the standard deviation of the parameters 1 to 12 by 10 percent in an OAT fashion decreases the minimum and typical liner lives of combustors A and B by less than two percent, as shown in Figures 4-9, 4-10, 4-11, and 4-11. The minimum life decreases by approximately 4 and 3 percent for combustors A and B, respectively, when the material property variability is decreased by 10 percent. Furthermore, increasing the material property variability has a negligible impact on the typical combustor life relative to the nominal. These results imply that loosening the manufacturing tolerances by 10 percent will not adversely impact the durability of the liner while improving the affordability of the part.

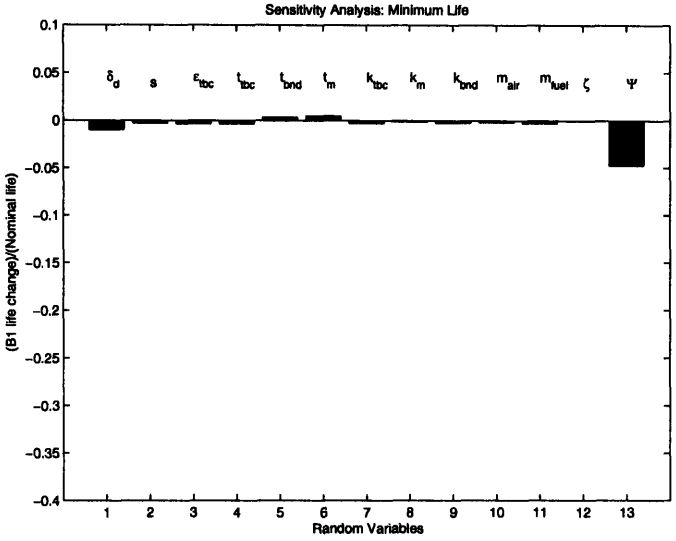

Figure 4-9: Combustor A: B_1 life change for 10 percent tolerance increase.

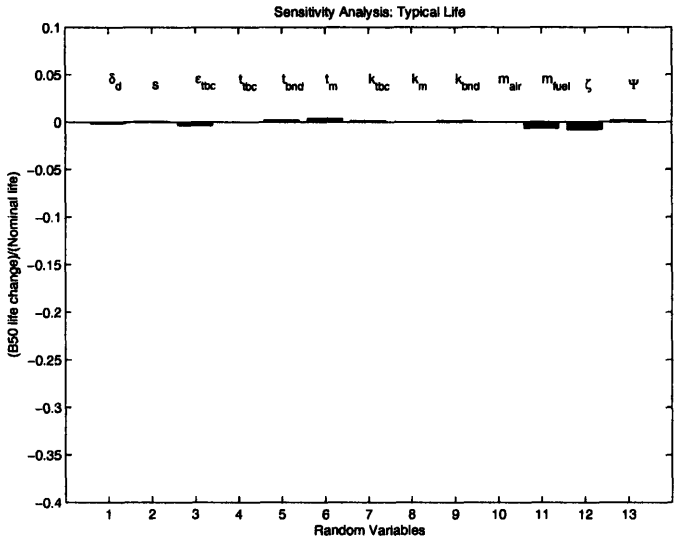

Figure 4-10: Combustor A: B_{50} life change for 10 percent tolerance increase.

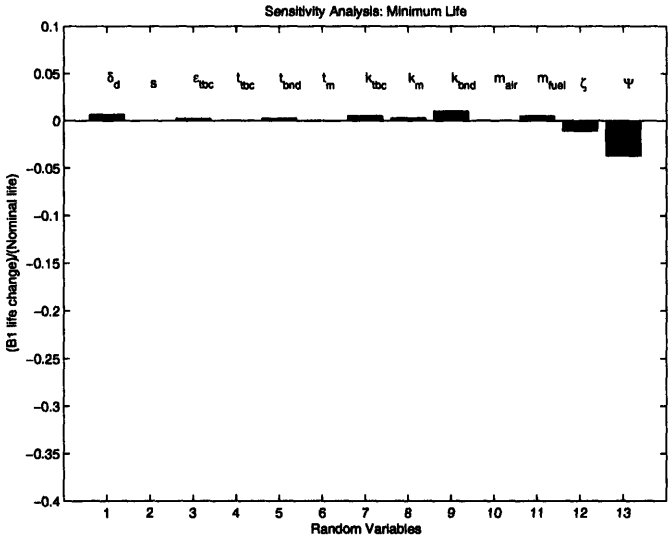

Figure 4-11: Combustor B: B_1 life change for 10 percent tolerance increase.

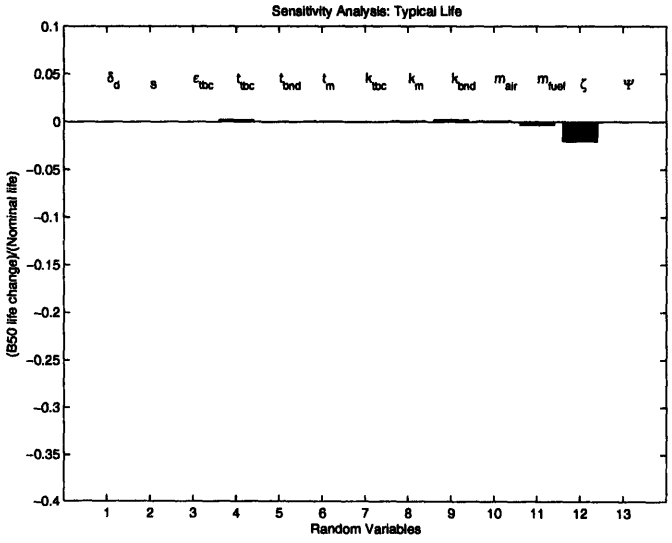

Figure 4-12: Combustor B: B_{50} life change for 10 percent tolerance increase.

4.5 Conclusions

The sensitivity analyses show that the leading drivers of the minimum combustor life and the typical combustor life are the material property variability and the combustor mixedness variability, respectively. A robust design that improves combustor liner durability would consist of a liner material with less material property variability than currently used on combustors A and B. Furthermore, a combustor configuration that increases the consistency of the combustor mixedness levels from cup to cup would decreases the liner temperature variability, and, in turn, would increase the typical combustor life. Increasing the manufacturing tolerances may improve the affordability of the combustor while satisfying the durability requirements. The results show that the life distributions of combustors A and B are insensitive to 10-percent tolerance increases of parameters 1 to 11. Increasing the manufacturing tolerances of parameters 1 to 10 may improve the affordability of the combustor while satisfying the durability requirements.

Chapter 5

Summary and Recommendations

5.1 Summary

This thesis has presented probabilistic and statistical techniques used to assess the impact of manufacturing variability on combustor liner durability.

- A probabilistic modeling framework that links the manufacturing variability of the liner, the fuel flow variability, and the dome air flow variability to the combustor liner temperature and combustor liner low-cycle fatigue life was presented. The effects of manufacturing variability were represented by 13 independent, normally-distributed random variables. A simplified combustor model, which consisted of a network flow analysis, a well-stirred reactor analysis, a lumped-parameter analysis of the combustor temperature field, a one-dimensional heat transfer analysis, and a low-cycle fatigue life analysis, was developed. The model was applied to two combustors used on commercial aircraft engines: A and B.

- The probabilistic assessment of the impact of fuel flow variability and air swirler flow variability on the outlet bulk gas temperature was conducted. The results showed that the probabilistic estimate of the outlet bulk gas temperature variability was consistent with rig test data provided by an engine company.

- The probabilistic model was used to assess the impact of manufacturing variability on the liner life distribution. A probabilistic analysis showed that a randomly selected combustor designed to the life predicted using deterministic methods may fail earlier than expected, and that the typical combustor life is 20 percent less than the nominal life for combustors A and B. Furthermore, the probabilistic estimate of the life distribution variability for combustor B was consistent with the variability in the field failure data. The material property variability accounted for 80 percent of the variability exhibited in the field failure data of combustor B.

- A sensitivity analysis showed that the material property variability and the combustor mixedness parameter were the leading drivers of the minimum combustor life and the typical combustor life, respectively. Moreover, opening the manufacturing tolerances by 10 percent by improve the affordability of the part while not impacting the combustor life.

5.2 Recommendations for Future Work

There are several opportunities for future work in the area of probabilistic analysis and design for gas turbine combustors. These areas include quantifying the impact of operational variability on combustor life, estimating the impact of manufacturing variability on hot streak migration, developing a physics-based model of the combustor mixedness levels, and applying a probability-based optimization of the combustion system. This section briefly describes these research opportunities.

5.2.1 Analytical Modeling of the Combustor Mixedness

The mechanisms that produce the cup-to-cup variability of the combustor mixedness should be identified. A possible source is the variability of the air flow swirler orientation at the front of the combustor [34]. Furthermore, the fuel injectors may be biased towards either the inner or outer liners. These biases are introduced during the combustor assembly process and lead to the variability of the fuel and air concentrations. This variability is manifested as the near-wall gas temperature variability referred to in this thesis.

5.2.2 Impact of Operational Variability on Combustor Liner Durability

The impact of operational variability on combustor liner durability was not accounted for in this thesis. Incorporating operability effects into the probabilistic analysis first requires a statistical model of the ambient temperature conditions for one or more fleets. These data would be incorporated into the block analysis presented in Chapter 3. Furthermore, the probabilistic analysis should be performed at several operating points. The analysis presented in this thesis, which is based on a hot-day, sea-level take-off operating point, provides a conservative estimate of the typical life. Thus, the likely effects of performing the probabilistic analysis at several operating points would be to increase the typical life estimate compared with the results presented in this thesis. Lastly, an assessment of the relative impact of the operational variability and the manufacturing variability on the combustor liner life should also be made.

5.2.3 Impact of Manufacturing Variability on Hot-Streak Migration

Hot streak migration through the combustor negatively impacts turbine durability [37]. These hot streaks chemically react in the turbine. They alter the heat transfer boundary conditions, increase the turbine blade temperatures, and decrease the blade oxidation life. A probabilistic analysis of the combustor chemical composition and temperature field would quantify the impact fuel flow variability and the inconsistency of the combustor mixedness on the migration of these fuel-rich streaks.

5.2.4 Probability-Based Combustion System Optimization

A probability-based optimization of the combustion system should be performed to assess whether a more robust configuration than current products can be attained. The optimization would be constrained by operability, durability, emissions, performance, weight, and affordability requirements while accounting for the effects of operational and manufacturing variability. The optimization would be applied to low-fidelity models that link the effects of operational and manufacturing variability to these design objectives.

5.2.5 Study of Material Property Variability versus Measurement Error

Future combustor durability studies should address the variability exhibited about the crack initiation life curve. The relative impact of material property variations and measurements error on the crack initiation life data has not been quantified. Incorporating both of these effects into the probabilistic analysis yielded a life distribution that was consistent with the combustor B field data. Directly modeling the effects of the material property variations is necessary in order to improve the precision of the combustor liner life estimate.

Appendix A

Crack Initiation Life Modeling

The life model presented in Chapter 2 consisted of a proprietary curve for the crack initiation life of Hastelloy-X. However, a more general model is needed if this curve is not available. This appendix presents an alternative approach for deterministically estimating the crack initiation life at a specified metal temperature.

A.1 Universal Slopes Method

The most widely used equation for estimating the number of cycles to crack initiation is shown in

$$\Delta\varepsilon_{total} = 3.5\frac{\sigma_{ult}}{E}N_f^{init^{-0.12}} + D^{0.6}N_f^{init^{-0.6}}. \tag{A.1}$$

It is commonly referred to as the Universal Slopes Method [49]. $\Delta\varepsilon_{total}$ is the total strain range. σ_{ult} is the ultimate tensile stress. E is the Young's Modulus. N_f^i is the number of cycles to crack initiation. D is the true fracture ductility. The total strain range is related to the alternating strain range, $\Delta\varepsilon_{alt}$, via Equation A.2.

$$\Delta\varepsilon_{alt} = \frac{1}{2}\Delta\varepsilon_{total} \tag{A.2}$$

The alternating strain is a function of the metal temperature, as shown in Equation A.3. In this equation, T_{mh} is the hot side metal temperature, T_{cool} is the film cooling air temperature, and α is the coefficient of thermal expansion. The metal temperature and the film cooling air temperature have units of degrees Fahrenheit.

$$\Delta\varepsilon_{alt} = \alpha(T_{mh} - T_{cool}) \tag{A.3}$$

The Young's Modulus, the ultimate tensile stress, and the true fracture ductility are also functions of the metal temperature. Data for the Young's Modulus and the ultimate tensile stress parameters were found in the 2003 Department of Defense Handbook [48]. The true fracture ductility curve was derived from elongation data found on the High Temp Metals, Inc. website [50]. Regression analyses were applied to these data in order to create response surfaces for these parameters. They are presented in the remaining parts of this appendix.

A.2 Young's Modulus

A response surface equation for the Young's Modulus is shown in

$$E = 29.8(10^7)\sum_{k=0}^{6}\beta_k \hat{T}_{mh}^k. \tag{A.4}$$

The regressors of this equation are given by

$$\begin{pmatrix} \beta_0 \\ \beta_1 \\ \beta_2 \\ \beta_3 \\ \beta_4 \\ \beta_5 \\ \beta_6 \end{pmatrix} = \begin{pmatrix} 0.8805 \\ -0.1052 \\ -0.0141 \\ -0.0012 \\ -0.0046 \\ 0.0011 \\ 0.0012 \end{pmatrix}. \tag{A.5}$$

The Young's Modulus has units of ksi. The metal temperature for this equation is scaled according to

$$\hat{T}_{mh} = \frac{T_{mh} - 903.1053}{557.6288}. \tag{A.6}$$

A.3 Coefficient of Thermal Expansion

A response surface for the coefficient of thermal expansion is shown in

$$\alpha = \sum_{k=0}^{6}\beta_k \hat{T}_{mh}^k. \tag{A.7}$$

Its regressors are given by

$$\begin{pmatrix} \beta_0 \\ \beta_1 \\ \beta_2 \\ \beta_3 \\ \beta_4 \\ \beta_5 \\ \beta_6 \\ \beta_7 \end{pmatrix} = \begin{pmatrix} 8.3785 \\ 0.4727 \\ -0.0318 \\ 0.0175 \\ -0.0096 \\ -0.0096 \\ -0.0016 \\ 0.0107 \end{pmatrix}. \tag{A.8}$$

Furthermore, the metal temperature is scaled according to Equation A.9. The coefficient of thermal expansion has units of inverse degrees Fahrenheit.

$$\hat{T}_{mh} = \frac{T_{mh} - 900}{447.2136} \tag{A.9}$$

A.4 Ultimate Tensile Stress

A response surface for the ultimate tensile stress is shown in Equation A.10.

$$\sigma_{ult} = \sum_{k=0}^{6} \beta_k \hat{T}_{mh}^k \tag{A.10}$$

Equation A.11 contains its regressors.

$$\begin{pmatrix} \beta_0 \\ \beta_1 \\ \beta_2 \\ \beta_3 \\ \beta_4 \\ \beta_5 \\ \beta_6 \end{pmatrix} = \begin{pmatrix} 0.8009 \\ -0.3470 \\ -0.2962 \\ -0.0144 \\ 0.1358 \\ 0.0139 \\ -0.0249 \end{pmatrix} \tag{A.11}$$

The metal temperature is scaled according to

$$\hat{T}_{mh} = \frac{T_{mh} - 1002.8}{615.8456}, \tag{A.12}$$

where the ultimate tensile stress has units of ksi.

A.5 Ductility

The ductility (D) is related to the elongation (ϵ) by

$$D = ln(1 + \epsilon). \tag{A.13}$$

The elongation is given as a function of temperature in [50]. The ductility was then estimated as a function of the metal temperature. Finally, a regression analysis was applied to the ductility data over a range of metal temperatures to yield

$$D = \sum_{k=0}^{4} \beta_k \hat{T}_{mh}^k, \tag{A.14}$$

where the regressor values are shown in

$$\begin{pmatrix} \beta_0 \\ \beta_1 \\ \beta_2 \\ \beta_3 \\ \beta_4 \end{pmatrix} = \begin{pmatrix} 1.6055 \\ 8.4255(10^{-4}) \\ -2.1506(10^{-6}) \\ 1.7619(10^{-9}) \\ 4.5058(10^{-13}) \end{pmatrix}. \tag{A.15}$$

A.6 Solution Procedure

Estimating the crack initiation life using this system of equations consists of a few steps. First, the user specifies the metal temperature. Then, the material properties are estimated using the response surfaces. In addition, the total strain range is determined using Equation A.3. Finally, Equation A.1 may be solved for the crack initiation life with a Newton-Raphson Method.

A.7 Crack Initiation Life Curve

The crack initiation life, as predicted by the Universal Slopes Method, is plotted against the metal temperature in Figure A-1. This figure shows that the crack initiation life is a strong function of the metal temperature. In particular, the crack initiation life decreases with increased metal temperature.

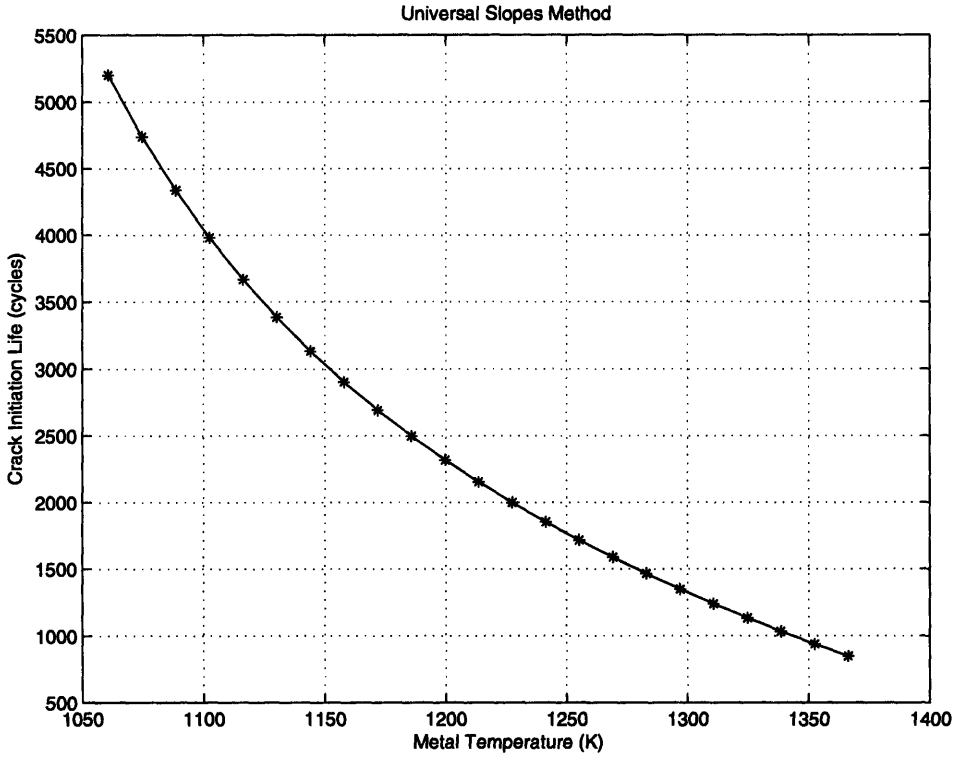

Figure A-1: Crack initiation life model: Universal Slopes Method

Appendix B

Crack Propagation Life Modeling

This appendix presents mathematical models for directly estimating the crack propagation life of Hastelloy-X. These models were used as part of the liner life analysis presented in Section 2.5.

B.1 Constant Temperature Crack Growth

Paris' Law, which is a model that quantifies the crack growth rate at specified temperature and stress states, is given by [29]

$$\frac{da}{dN_f^p} = C_1 \Delta K^{C_2}, \tag{B.1}$$

where a is the crack length. N_f^p is the crack propagation life. ΔK is the stress intensity factor. C_1 and C_2 are the constant at for a specified metal temperature. The stress intensity factor is estimating using Equation B.2

$$\Delta K = \sigma_{vm} \sqrt{\pi a} Y, \tag{B.2}$$

where σ_{vm} is the equivalent stress and Y is a numerical correction factor.Y is a function of the of the crack size and the specimen width, W, as shown in Equation B.3 [26].

$$Y = \frac{1}{\sqrt{\pi}}(1.986 + 1.782(\frac{a}{W}) + 6.998(\frac{a}{W})^2 - 21.505(\frac{a}{W})^3 + 43.351(\frac{a}{W})^4 \tag{B.3}$$

The low-cycle fatigue life of a combustor is reached when one of two conditions are met. Condition I occurs when the crack size exceeds a maximum allowable length. The crack propagation life is analytically estimated using Equation B.4.

$$N_f^p = \int_{a_{initial}}^{a_{final}} \frac{da}{C_1 \Delta K^{C_2}} \tag{B.4}$$

The integration occurs between a starting crack size and the maximum allowable crack length. The initial crack size may defined as the "smallest crack of engineering significance" [52]. Manson stated that this crack size is approximately 0.003 inches. This estimate is based on the application of ultrasonic techniques to detect cracks of this size. The maximum crack size is set by the part specifications.

Condition II, also known as the fast fracture condition, occurs when the stress intensity factor surpasses the fracture toughness of the part [29]. Fast fracture is the growth of existing cracks at the speed of sound. The fracture toughness, a material property, is a function of the metal temperature. The fracture toughness at a specified temperature may be estimated a priori. Then, the integration of Paris' Law is performed until condition II is met. Finally, the number of cycles-to-failure at which this occurs is defined as the crack propagation life.

B.2 Variable Temperature Crack Growth

The temperature dependencies of C_1 and C_2 must be accounted for when there is metal temperature variability. Equations B.5, B.6, B.7, and B.8 comprise a model for the crack growth.

$$\frac{da}{dN_f^p} = \beta_1 \tag{B.5}$$

$$ln(\beta_1) = ln(A) + \frac{\beta_0}{T_{mh}} \tag{B.6}$$

$$ln(A) = -4.1 - 0.1617\Delta K + 0.0095\Delta K^2 - 1.333(10^{-4})\Delta K^3 \tag{B.7}$$

$$\beta_0 = -1.0 - 0.1733\Delta K + 0.0075\Delta K^2 - 1.1667(10^{-4})\Delta K^3 \tag{B.8}$$

These equations were created from the research of D. Jablonski [26] on the fatigue behavior of Hastelloy-X at elevated temperatures. In particular, regression analysis were applied to data for the Hastelloy-X fatigue at various metal temperatures. These equations must be numerically integrated in order to solve for the crack propagation life at a variety of temperatures.

Appendix C

JP-8 Chemical Kinetic Mechanism

This appendix presents a chemical kinetic mechanism for the chemical reaction

$$\phi C_n H_m + (n + \frac{m}{4})(O_2 + 3.76N_2) \rightharpoonup \nu_{CO_2} CO_2 + \nu_{H_2O} H_2O + ... + (n + \frac{m}{4})(3.76)N_2 \quad \text{(C.1)}$$

where jet fuel is represented by the molecule $C_n H_m$ for $n = 12$ and $m = 23$ and ϕ is the equivalence ratio. The mechanism is implemented in CHEMKIN III to estimate the temperature and composition of the combustion products.

C.1 Chemical Mechanism

A chemical kinetic mechanism for JP-8 was proposed by Mawid, et. al. [41], and it was used to determine the bulk gas temperatures. The mechanism is shown in Table C.1. It contains 13 species and 20 steps. The species are $C_{12}H_{23}$, C_2H_2, H_2, CO, O_2, O, OH, H, H_2, NO, CO_2, N, and N_2. M represents a third body.

C.2 Reaction Rate Constant

The rate of each reaction (k) is determined from the Arrhenius law [53]. This law states that colliding molecules which contain energy greater the activation energy will react. This phenomenon is characterized by

$$k = AT^b \exp\left(-\frac{E}{RT}\right), \quad \text{(C.2)}$$

where E is the activation energy of the reaction, R is the universal gas constant,and T is the gas temperature. A and b are empirical constants. The first term of the equation (AT^b) represents the effects of the collision frequency. The second term $\exp -(\frac{E}{RT})$ is called the Boltzmann factor. It quantifies the proportion of collisions containing energy exceeding the activation energy. A has units of mole-cm-sec-K. E has units of cal/mole.

Table C.1: JP-8 Chemical Kinetic Mechanism

STEP	REACTION	A	b	E
1	$2C_{12}H_{23} => 12C_2H_2 + 11H_2$	4.21E+14	0.1	29200.0
2	$C_2H_2 + O_2 => 2CO + H_2$	1.21E+13	0.1	30200.0
3	$CO + O + M = CO_2 + O => CO_2 + M$	6.17E+14	0.0	3000.0
4	$CO + O_2 = CO_2 + O$	1.60E+13	0.0	41000.0
5	$CO + OH = CO_2 + H$	1.51E+07	1.3	-758.0
6	$OH + H_2 = H_2O + H$	1.17E+09	1.3	3626.0
7	$O + OH = O_2 + H$	4.00E+14	-0.5	0.0
8	$O + H_2 = OH + H$	5.06E+04	2.7	6290.0
9	$2OH = O + H_2O$	6.00E+08	1.3	0.0
10	$2H + M = H_2 + M$	1.00E+18	-1.0	0.0
11	$H + OH + M = H_2 + M$	1.60E+19	-2.0	0.0
12	$H + O + M = OH + M$	1.10E+17	-0.6	0.0
13	$2O + M = O_2 + M$	1.89E+13	0.0	-1788.0
14	$N + NO = N_2 + O$	3.27E+12	0.3	0.0
15	$N + O_2 = NO + O$	6.40E+09	1.0	6280.0
16	$N + OH = NO + H$	3.80E+13	0.0	0.0
17	$H_2 + O_2 = 2OH$	1.70E+13	0.0	47780.0
18	$2H + H_2 = 2H_2$	9.20E+16	-0.6	0.0
19	$2H + H_2O = H_2 + H_2O$	6.00E+19	-1.3	0.0
20	$2H + CO_2 = H_2 + CO_2$	5.49E+20	-2.0	0.0

Appendix D

Probability Fundamentals

The section presents some fundamental concepts of probability. First, the random variable concept and its main descriptors are presented. Then, three probability distributions are presented: the Gaussian, the log-normal, and the Weibull distributions.

D.1 Random Variables

Random variables numerically identify a range of possible outcomes for a random phenomenon [24]. These parameters are often characterized by two main descriptors. They are the first and second moments of the random variable. The first moment of a random variable, x provides a weighted average of the values in x. It is the expected value of x. The expected value is determined from

$$E[x] = \int_{-\infty}^{\infty} x f_x(x) dx. \tag{D.1}$$

The expected value, also referred to as the mean value (μ), is shown determined from

$$\mu_x = E[x]. \tag{D.2}$$

In Equation D.1, $f_x(x)$ is the probability density function (PDF) of x. The PDF is related to the cumulative distribution function (CDF), $F_x(x)$, in

$$F_x(x) = \int_{-\infty}^{x} f_x(x) dx. \tag{D.3}$$

The CDF quantifies the probability content between $-\infty$ and x.

The second descriptor estimates the level of variability about the mean value. This descriptor is the second central moment, or variance, as determined from

$$Var[x] = \int_{-\infty}^{\infty} (x - \mu_x)^2 f_x(x) dx. \tag{D.4}$$

Another measure of the variability level of x is the standard deviation. The standard deviation is estimated by taking the square root of the variance, as shown in

$$\sigma_x = \sqrt{Var[x]}. \tag{D.5}$$

D.2 Gaussian Distribution

The Gaussian, or normal, distribution is the most widely used probability density function [24]. The Gaussian describes most naturally occurring phenomena. In this thesis, the normal distribution is used to mathematically model the effects of manufacturing variability on key combustor design parameters. For a random variable x that is represented by a normal distribution, the PDF is given by

$$f_x(x) = \frac{1}{\sqrt{2\pi\sigma}} \exp\left(\frac{1}{2}\left(\frac{x-\mu}{\sigma}\right)^2\right) \tag{D.6}$$

and the CDF ($F_x(x)$) is defined by

$$F_x(x) = \frac{1}{\sqrt{2\pi\sigma}} \int_{-\infty}^{x} \exp\left(\frac{1}{2}\left(\frac{x-\mu}{\sigma}\right)^2\right). \tag{D.7}$$

D.3 Log-normal Distribution

The log-normal distribution is applicable to random variables that are always positive. Some applications include the strength and fatigue life of a material, rainfall intensity, project completion time, and air traffic volume [24]. The PDF of a logarithmic normal, or log-normal, distribution for a random variable x is shown in

$$f_x(x) = \frac{1}{\sqrt{2\pi\zeta x}} \exp -\frac{1}{2}\left(\frac{lnx-\lambda}{\zeta}\right)^2. \tag{D.8}$$

The natural logarithm of x is normal if x has log-normal distribution. The parameters λ and ζ are the mean and standard deviation of the natural logarithm of x, as shown in

$$\lambda = E(lnx) \tag{D.9}$$

and

$$\zeta = \sqrt{Var(lnx)}. \tag{D.10}$$

D.4 Weibull Distribution

The Weibull distribution, named after Swedish engineer Wallodi Weibull (1887-1979), is widely used in engineering problems. In particular, it is used in reliability engineering to estimate the probability distribution of parts where there are multiple failure sites. The life of this part is defined by the site with the lowest life. In other words, these failures are governed by the weakest link [39].

The Weibull CDF ($F_x(x)$) for a random variable, x, is determined from

$$F_x(x) = 1 - \exp\left[-\left(\frac{x}{\alpha}\right)^{\beta}\right]. \tag{D.11}$$

$F_x(x)$ is related to two constants, α and β. The significance of α and β is more readily determined from the hazard function, which quantifies the failure rate for a given density distribution. The hazard function, $h(x)$, is related to the PDF and CDF of x via

$$h(x) = \frac{f(x)}{1 - F(x)}. \tag{D.12}$$

The PDF can be determined from the CDF using Equation D.13.

$$f(x) = \frac{dF}{dx} \tag{D.13}$$

Substituting Equations D.11 and D.13 into Equation D.12 yields an expression for the hazard function, as shown in

$$h(x) = \frac{\beta}{\alpha}(\frac{x}{\alpha})^{\beta-1}. \tag{D.14}$$

α scales the distribution of x in the hazard function and is called the scale parameter. β determines the shape of the hazard function [45] of x and is called the shape function. β also determines the slope of distribution of x on a Weibull probability scale. Lower values of β indicate that x contains more variability than higher values.

Bibliography

[1] A. Lefebvre, *Gas Turbine Combustion*. Taylor Francis. 1999.

[2] J.C. Bailey, J. Intile, T.F. Fric, A.K. Tolpadi, A.K. Nirmalan, and R.S. Bunker, *Experimental and Numerical Study of Heat Transfer in a Gas Turbine Combustor Liner.* ASME Journal of Engineering for Gas Turbines and Power. Vol. 125. October, 2003.

[3] W.J. Dodds and D.W. Bahr, *Combustion System Design*. Notes.

[4] C. Lykins, D. Thompson, and C. Pomfret, The Air Force's Application of Probabilistics to Gas Turbine Engines, AIAA paper 94-1440-CP.

[5] H.O. Madsen, *"Fatigue Reliability of Marine Structures,"* Stochastic Approach to Fatigue, edited by K. Sobczk, Springer-Verlag, New York, 1993.

[6] H. Millwater, Y.T. Wu, Y. Trong, D. Riha, and C. Leung, *"Recent Developments of the NESSUS Probabilistic Structural Analysis Computer Program,"* AIAA Paper 92-2411, 1992.

[7] G.H. Besterfield, W.K Liu, M.A. Lawrence, and T. Belytschko, *"Fatigue Crack Growth Reliability by Probabilistic Finite Elements,"* Computer Methods in Applied Mechanics and Engineering, Vol. 86, 1991, pp. 297-320.

[8] C.H. Juang and S.H. Yang, *Characterization of the Uncertainty of the Robertson and Wride Model for Reliability Analysis of Soil Liquefaction.*

[9] X. Yu, K. Chang, K.K. Choi, *Probabilistic Structural Durability Prediction,"* AIAA Journal, Vol. 36, No.4, April 1998.

[10] M.S. Eldred, H. Agarwal, V.M. Perez, S.F. Wojtkiewicz, Renaud, J.E. *"Investigation of Reliability Method Formulations in DAKOTA/UQ.*

[11] W.F. Wu and C.C. Ni, *Probabilistic models for fatigue crack propagation and their experimental verification.* Probabilistic Engineering Mechanics. February, 2004.

[12] V.E. Garzon and D.L. Darmofal, *Impact of Geometric Variability on Axial Compressor Performance.* ASME Journal of Turbomachinery, Vol. 125, No.4, pp. 692-703, October 2003.

[13] V. Sidwell and D. L. Darmofal, *The Impact of Blade-To-Blade Variability and Assembly on Turbine Cooling Performance.* ASME Journal of Turbomachinery, Vol. 127, No. 4, pp. 763-770, October 2005.

[14] D. Mavris and B. Roth, *'A Methodology For Robust Design of Impingement Cooled HSCT Combustor Liners'*. AIAA 1997.

[15] J. Palladino, Personal communication. MIT. 2004.

[16] M. A. Mawid, et al., Development and Validation of Detailed and Reduced Chemical Kinetic Mechanisms for Oxidation of JP-8/Jet-A/JP-7 Fuels. ISABE-2003-1028.

[17] CHEMKIN III. Reaction Design. 1999.

[18] P. Gosselin, A de Champlain, and D. Kreschmer, *Prediction of Wall Heat Transfer for a Gas Turbine Combustor.* Proc. Instn. Mech. Engrs. Vol. 213, Part A, 1999.

[19] J. Monty, Personal communication. GE Aircraft Engines. 2003.

[20] D.R. Ballal and A.H. Lefebvre, *Film-Cooling Effectiveness in the Near Slot Region.* Journal of Heat Transfer, pp. 265-266, 1973.

[21] Handbook of Heat Transfer. page 5-29.

[22] W. M. Rohsenow *Handbook of Heat Transfer.* Third Edition. McGraw-Hill Handbooks. 1998.

[23] H. Abramson. GE Aircraft Engines. 2005.

[24] A. Ang and W. Tang, Probability Concepts in Engineering Planning and Design: Volume I - Basic Principles. John Wiley Sons, Inc. 1975.

[25] H.L. Foltz and M. J. Kenworthy, *A Procedure for Evaluating Fuel Composition Effects on Combustor Life.* ASME, 82-GT-296.

[26] D. A. Jablonski, *Fatigue Behavior of Hastelloy-X at Elevated Temperatures in Air, Vacuum, and Oxygen Environments.* MIT Ph.D. Thesis. Department of Materials Science and Engineering. 1978.

[27] M.F. Modest, *Radiative Heat Transfer.* McGraw Hill, 1999.

[28] A.F. Mills, *Basic Heat Mass Transfer, Second Edition.* Prentice Hall, Inc. 1999.

[29] M.F. Ashby and D.R.H. Jones, *Engineering Materials I: An Introduction To Their Properties Applications.* Second Edition. Butterworth-Heinemann.

[30] S.M. Spearing, Personal communication. 2005.

[31] J. Starkweather, Personal communication. 2006.

[32] S. Stephens and M. Shaw, Personal communication. GE Aircraft Engines. 2004.

[33] A. Mascarenas, Personal communication. Delta Airlines. 2004.

[34] A. Currin, Personal communication. GE Aircraft Engines. 2004.

[35] D.C. Montgomery, *Design and Analysis of Experiments: Second Edition.* John Wiley Sons. 1984.

[36] A. Ghoniem, *2.28 Course Notes.* Spring 2003.

[37] D.R. Kirk, *Near-Wall Reaction Effects on Film-Cooled Surface Heat Transfer.* Ph.D. Thesis, Massachusetts Institute of Technology. August 2002.

[38] Lapeyre, Pardoux, and Sentis., *Introduction to Monte Carlo Methods for Transport and Diffusion Equations.* Oxford University Press. 1998.

[39] E. Suhir, *Applied Probability for Engineers and Scientists.* McGraw-Hill. 1997.

[40] E. Chong and S. Zak, *An Introduction to Optimization, Second Edition.* John Wiley Sons. 2001.

[41] M.A. Mawid, T.W. Park, B. Sekar, and A. Arana, *Development and Validation of Detailed and Reduced Chemical Kinetic Mechanisms for Oxidation of JP-8/Jet-A/JP-7 Fuels.* ISABE-2003-1028.

[42] W. Weibull, *A Statistical Distribution Function of Wide Applicability.* Transactions of the Americal Society of Mechanical Engineers. September, 1951. Pages 293-297.

[43] P. Gosselin, A. de Champlain, and D. Kretschmer, *Prediction of Wall Heat Transfer for a Gas Turbine Combustor.* Proc. Instn. Mech. Engrs. Vol. 213, Part A. 1999.

[44] A.H. Lefebvre, *Influence of Fuel Properties on Gas Turbine Combustion Performance.* AFWAL-TR-84-2104, 1985.

[45] http://www.mathpages.com/home/kmath122/kmath122.htm

[46] E. Lada, K. Wagner, M. Steiger, M. Natalie, J.R. Wilson, *Introduction to Modeling and Generating Probabilistic Input Processes for Simulation.* Proceedings of the 2005 Winter Simulation Conference.

[47] J. Barraquad and D. Martineau, *Numerical Valuation of High Dimensional Multivariate American Securities.* Journal of Financial and Quantitative Analysis, Vol. 30, No. 3. Sep., 1995, pp. 383-405.

[48] Metallic Materials and Elements for Aerospace Vehicle Structures. Department of Defense Handbook. MIL-HDBK-5J. January, 2003. Chapter 6, pp 21-26.

[49] A. Kountras, *Probabilistic Analysis of Turbine Blade Durability.* S.M. Thesis, Massachusetts Institute of Technology, 2004.

[50] http://www.hightempmetals.com/techdata/hitempHastXdata.php

[51] T.L. Anderson, *Fracture Mechanics: Fundamentals and Applications.* CRC Press. 1995.

[52] S.S. Manson, *Fatigue: A Complex Subject - Some Simple Approximations.* The William M. Murray Lecture, 1964.

[53] K.K. Kuo, *Principles of Combustion.* John Wiley Sons. 1986.